

## **RESEARCH ARTICLE**

# A tale of two fish tails: does a forked tail really perform better than a truncate tail when cruising?

Nils B. Tack\*,‡ and Brad J. Gemmell

#### **ABSTRACT**

Many fishes use their tail as the main thrust producer during swimming. This fin's diversity in shape and size influences its physical interactions with water as well as its ecological functions. Two distinct tail morphologies are common in bony fishes: flat, truncate tails which are best suited for fast accelerations via drag forces, and forked tails that promote economical, fast cruising by generating lift-based thrust. This assumption is based primarily on studies of the lunate caudal fin of Scombrids (i.e. tuna, mackerel), which is comparatively stiff and exhibits an airfoil-type cross-section. However, this is not representative of the more commonly observed and taxonomically widespread flexible forked tail, yet similar assumptions about economical cruising are widely accepted. Here, we present the first comparative experimental study of forked versus truncate tail shape and compare the fluid mechanical properties and energetics of two common nearshore fish species. We examined the hypothesis that forked tails provide a hydrodynamic advantage over truncate tails at typical cruising speeds. Using experimentally derived pressure fields, we show that the forked tail produces thrust via acceleration reaction forces like the truncate tail during cruising but at increased energetic costs. This reduced efficiency corresponds to differences in the performance of the two tail geometries and body kinematics to maintain similar overall thrust outputs. Our results offer insights into the benefits and tradeoffs of two common fish tail morphologies and shed light on the functional morphology of fish swimming to guide the development of bio-inspired underwater technologies.

KEY WORDS: Fish swimming, Caudal fin, Efficiency, Performance, Cruising, PIV

#### INTRODUCTION

The caudal fin acts as the primary thrust producer in many fish species and exhibits a range of morphologies. From early empirical studies on form and function (Breder, 1926; Webb, 1978a) to more recent mechanical and computational studies of the propulsive properties of the tail (Borazjani and Sotiropoulos, 2009; Esposito et al., 2012; Krishnadas et al., 2018; Lauder, 2014; Song et al., 2021), morphology has pronounced effects on the nature and magnitude of the forces produced during undulatory swimming. These functional attributes play an integral role in the swimming

Department of Integrative Biology, University of South Florida, 4202 East Fowler Avenue, Tampa, FL 33620, USA

<sup>&</sup>lt;sup>‡</sup>Author for correspondence (nils\_tack@brown.edu)



N B T 0000-0002-5399-4788

\*Present address: School of Engineering, Brown University, 345 Brook Street,

speeds over 4 body lengths per second (BL s<sup>-1</sup>) (Blaxter, 1969; Magnuson, 1970). Because the power required to overcome drag increases with the cube of the swimming speed, the range at this cruising speed is limited (Weihs, 1973b). Long-range cruising speeds are generally lower, at about 1.3–1.7 BL s<sup>-1</sup>, to minimize the net cost of transport and maximize the range (Blank et al., 2007; Magnuson, 1966; Weihs, 1973b). The basis of our knowledge about the propulsive properties of

performance of fishes (Blake, 2004; Fletcher et al., 2014; Helfman et al., 2009; Lauder, 2000). During long-duration swimming and

cruising, they can regulate the overall energetic efficiency by

appreciable amounts (Blake, 2004; Weihs, 1973b). Early studies on

fish energetics indicate that some fishes can cruise at swimming

body/caudal fin swimming comes in part from the study of two typical fin morphologies: a generic triangular (truncate) caudal fin and a forked caudal fin (Bainbridge, 1963; Blake, 2004; Gibb et al., 1999; Lauder, 2000). Forked caudal fins have a high aspect ratio given that they are tall with a proportionally small surface area. High aspect ratio tails have evolved convergently in several fast-cruising species, including tunas, mackerels, billfishes, some sharks, marine mammals such as dolphins, and the extinct reptilian ichthyosaur (Fletcher et al., 2014; Helfman et al., 2009). Conversely, many species performing fast accelerations and turning maneuvers, such as salmons, trouts, snappers, groupers and cods, exhibit low aspect ratio truncate tails (Frith and Blake, 1995; Webb, 1978a). Traditionally, fishes' ecology and performance were associated with their caudal fin morphology. The current paradigm found in textbooks (e.g. Helfman et al., 2009) and reported in reviews of fish locomotion (Blake, 2004; Fletcher et al., 2014; Lauder, 2000; Sfakiotakis et al., 1999) highlights how high aspect ratio forked tails are ideal for economical sustained swimming while truncate tails are best suited for rapid accelerations. Behind this fundamental concept is the idea that by discarding the central portion of the tail, the forked morphology reduces drag from the body wake, thus limiting the energy demand during prolonged swimming (Fletcher et al., 2014; Helfman et al., 2009; Lauder, 2000). Functional and design constraints identified by Webb (1978a,b) corroborate this interpretation that functional requirements for high performance during cruising generally conflict with demands for high accelerations in unsteady locomotion.

However, most of our current knowledge about forked tails comes from the study of the stiff and sickle-shaped lunate tail, a specialized form of the forked tail with a high aspect ratio that experiences minimal drag (Borazjani and Daghooghi, 2013; Brücker and Bleckmann, 2010; Song et al., 2021; White et al., 2021). This forked morphology produces thrust through lift forces similar to insect flight that maintains a low-pressure zone along the propulsor (Borazjani and Daghooghi, 2013; Dickinson, 1996; Dickinson et al., 1999). Conversely, low aspect ratio truncate tails increase the pressure along the fin surface to produce thrust via acceleration reaction forces (Frith and Blake, 1995; Webb, 1978a).

Providence, RI 02912, USA.

Because the larger surface area of truncate tails induces more drag relative to lunate tails, they are reported to perform weakly at cruising speeds (Lauder, 2000). However, this generalized pattern does not consider species with forked – but not lunate – caudal fins. This contrast is important because numerically dominant species of many fish genera and families such as *Chromis*, Carangidae (e.g. pompano, trevally, jack), Clupeidae (e.g. herring, sardine) and Engraulidae (e.g. anchovy) exhibit the forked, non-lunate fin type.

Many fishes move efficiently through water with a low cost of transport (Breder, 1926; Graham and Dickson, 2004; van Ginneken et al., 2005). As a result, there is a growing interest in the bioinspired design of fish-based underwater machines (Lauder et al., 2012; Wainwright and Lauder, 2020; Wang et al., 2019a; White et al., 2021). This has led to several studies that employed both mechanical and theoretical models that have advanced our understanding of how contrasting tail morphologies may confer different functional advantages (Feilich and Lauder, 2015; Krishnadas et al., 2018; Liu and Dong, 2016). However, comparative investigations of forked versus truncate tail shapes using live fish have not been conducted. Live animal comparisons are essential given the complex mechanical and morphological subtleties associated with a propulsive control surface innervated with independently controlled fin rays. While in some cases, elaborate tail fin morphologies can result from sexual selection (Offen et al., 2008; Reznick et al., 2021), we are considering only non-sexually dimorphic species from the perspective of locomotor modalities.

In this study, we selected mojarras (Eucinostomus argenteus) and pinfish (Lagodon rhomboides) because they are comparable in several ways. They are cohabitating species found along sandy beaches and shallow inshore habitats subject to tidal flows (Eschmeyer and Herald, 1999; Hansen, 1969). Neither species is known to school (Eschmeyer and Herald, 1999; Nelson, 2002) and they display comparable body plans and sizes (see Supplementary Materials and Methods, 'Comparison of Mojarra and Pinfish', and Fig. S1). Both species feed on small invertebrates (Carr and Adams, 1973; Kerschner et al., 1985), but pinfish exhibit ontogenetic changes in diet and demonstrate omnivory, carnivory (including small fishes) and herbivory at different times, locations and stages of development (Stoner, 1980). Mojarras and pinfish are characterized by their distinct forked (non-lunate) and truncate caudal fins. respectively (Fig. 1). Here, we sought to isolate the effects of particular caudal fin shapes to address the question: does a forked geometry convey a significant advantage at cruising speeds? In this investigation, we compared the fluid flow patterns and pressure fields on the surface of the fins to determine, experimentally, the influence of tail shape on the overall performance and energetic cost of cruising. Given our current knowledge about the functional attributes of the caudal fins of fishes, we hypothesized that the forked tail of mojarras would demonstrate lift-based propulsion with lower energetics costs compared with the drag-based truncate tail of pinfish. Here, we provide new evidence to explain the phenotypic divergence of these two tail geometries and show potential limitations of generalizing tail shape and function.

# MATERIALS AND METHODS Animals

We collected silver mojarras (*Eucinostomus argenteus* Baird & Girard 1855) and pinfish [*Lagodon rhomboides* (Linnaeus 1766)] from the Tampa Bay area (W. Courtney Campbell Causeway, Tampa, FL, USA, and Weedon Island Preserve, St Petersburg, FL, USA). The fish were housed singly in 38 l aquariums maintained at 21°C, with a salinity of 30% and 12 h:12 h light:dark photoperiod

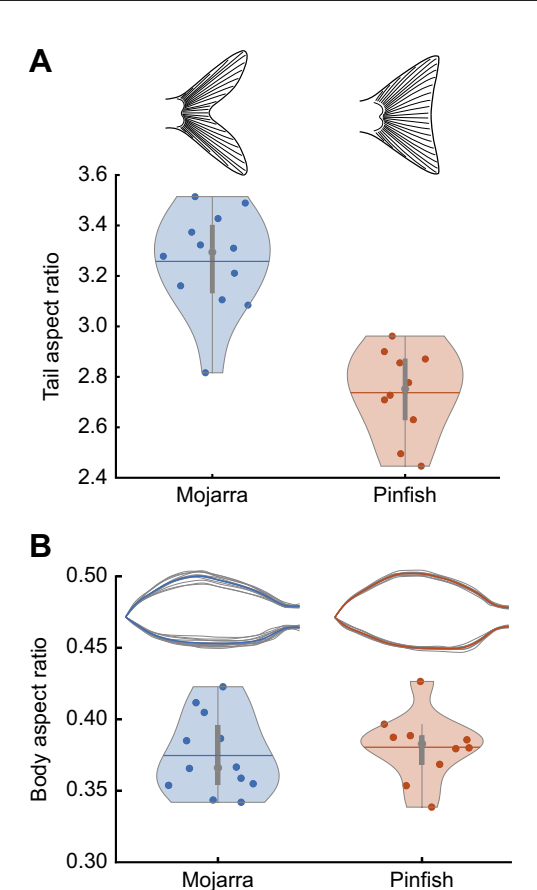


**Fig. 1.** Caudal fin and body aspect ratios of mojarras and pinfish.

(A) The aspect ratio of the two tail morphologies was statistically different (mojarra: *n*=12 fish, pinfish: *n*=10 fish, *U*-test, *P*<0.001). (B) Mojarras and pinfish have comparable body aspect ratios (*U*-test, *P*=0.531). Silhouettes of all the specimens from the lateral view indicating body depth are shown. All measurements are shown in gray. The mean silhouette for both species is also shown. The gray dot in the violin plots indicates the mean, and the horizontal line is the median. Shading represents the kernel density estimate for the data.

to ensure individuals could be distinguished. The fish were fasted for 24 h prior to any experiment. Once placed in the swim tunnel, the animals were acclimated at a swimming speed <0.3 BL s<sup>-1</sup> for 4 h in fully aerated and thermoregulated water (21±1.0°C). All experiments were conducted in accordance with the laws of the State of Florida and under IACUC protocols (permit no. IS00005965) approved by the University of South Florida (Tampa). Using ImageJ software, we digitally measured standard BL along the midline of each specimen from scaled dorsal view images. The aspect ratio of the body of mojarras and pinfish - representative of the cross-sectional area of the fish subject to the flow – was obtained from scaled lateral and dorsal views of each specimen to confirm the similarity in body shape (see Supplementary Materials and Methods, 'Comparison of Mojarra and Pinfish', and Fig. S1). The aspect ratio of the tail was calculated as the square of the span of the fin (the distance between the superior and inferior tips of the caudal fin) divided by the surface area of the fin (Fig. S1). The surface area of the fin was measured digitally for both species from lateral view images of the fish (see Supplementary Materials and Methods and Fig. S1).

#### Swim tunnel and respirometry

We used a modified acrylic 5 l Brett-type swim tunnel respirometer (Loligo Systems, Viborg, Denmark). Individual fish naturally swam

steadily at the center of the test section during swim trials. The working section of the swim tunnel was  $30\times7.5\times7.5$  cm (length×width×depth). The flume was submerged in an aerated outer buffer tank maintained at ambient temperature ( $21\pm1.0^{\circ}$ C). We assessed flow characteristics in the test section using particle image velocimetry (PIV) to ensure a uniform velocity profile throughout the cross-sectional area of the test section.

Relative oxygen consumption rates  $(\dot{M}_{\rm O_2})$  were measured for swimming speeds ranging from 0.25 BL s<sup>-1</sup> to 2.5 BL s<sup>-1</sup> for mojarras and 0.5 BL s<sup>-1</sup> to 3.0 BL s<sup>-1</sup> for pinfish. We employed intermittent flow respirometry derived from existing methods to limit the risks of hypoxia and hypercapnia (Tack et al., 2021). In summary, each measurement period consisted of two distinct phases: (1) a measurement period of 10 min (for all swimming speeds) during which the swim tunnel was sealed; and (2) a flush period during which oxygen saturation was brought to 100% using fully aerated, filtered and thermoregulated artificial seawater from the external buffer tank. Temperature-corrected dissolved oxygen concentration was measured in mg l<sup>-1</sup> using an optical oxygen dipping probe (PreSens, DP-PSt3, Regensburg, Germany) connected to a fiber-optic oxygen transmitter (PreSens, OXY-1 SMA) interfaced to a computer. The rate of oxygen consumption  $(\dot{M}_{\rm O_2})$  was calculated as follows:

$$\dot{M}_{\rm O_2} = \frac{(\Delta[{\rm O_2}] - \Delta[{\rm O_2}]_{\rm background}) \times V}{m},\tag{1}$$

where oxygen consumption is measured in mg min<sup>-1</sup> kg<sup>-1</sup>,  $\Delta$ [O<sub>2</sub>] is the total decline in oxygen concentration in the swim tunnel respirometer over a measurement period of 10 min,  $\Delta$ [O<sub>2</sub>]<sub>background</sub> is the change in oxygen concentration due to bacterial background respiration, V is the respirometer water volume (5.48×10<sup>-3</sup> m³), and m is the mass of the fish in kg. Cost of transport (COT; J m<sup>-1</sup> kg<sup>-1</sup>) serves as a measure of swimming efficiency and was calculated using  $\dot{M}_{\rm O_2}$  and the resting oxygen consumption rate ( $\dot{M}_{\rm O_2,resting}$ ) as follows:

$$COT = \frac{\dot{M}_{O_2} - \dot{M}_{O_2, resting}}{U}, \tag{2}$$

where U is the swimming speed in m s<sup>-1</sup> at each velocity increment. Conversion of metabolic respiration to energy expended (J) is accomplished by using the oxy-calorific equivalent of 3.24 cal mg<sup>-1</sup> of  $O_2$  measured for carnivorous fish (Elliott and Davison, 1975) and the standard thermochemical conversion factor 4.184 J cal<sup>-1</sup>.

## Flow visualization

We selected the cruising speed *U*=1.5 BL s<sup>-1</sup> as it corresponded to the swimming speed at which the COT of both the mojarras and the pinfish was near their respective minima (see Supplementary Materials and Methods). We used high-speed 2D PIV to obtain velocity fields around the fish's body and caudal fin. Recordings were acquired by a high-speed, high-resolution digital video camera (Fastcam Mini WX 100, Photron, Tokyo, Japan) at 1000 frames s<sup>-1</sup> (2048×2048 pixels). For horizontal (frontal) planar transections, 10 μm hollow glass seeding particles (Potter Industries, Malvern, PA, USA) were illuminated by two opposing overlapping horizontal laser sheets produced by two continuous-wave 808 nm lasers (MDL-H-808 3000–6000 mW, OptoEngine LLC, Midvale, UT, USA) to eliminate shadows on either side of the fish. For vertical planar transections of the tail (posterior view), a single vertical laser sheet was produced by a continuous-wave 532 nm laser

(OptoEngine LLC). A narrow mirror was mounted downstream of the swimming fish at a 45 deg angle to project the posterior view of the tail to the camera mounted above (Fig. S2). Given the challenges and uncertainty of multi-plane data using live fish (Lauder and Madden, 2007) and the focus on the forked region of the tail, we investigated a single plane located 2/3 of the tail length from the caudal peduncle. The presence of the mirror downstream of the test section lowered bulk flow velocity slightly compared with the horizontal transection setup without the mirror. Thus, the calibration of water flow velocity to the voltage output from the external motor generating the flow in the respirometer was performed using PIV to match the flow conditions obtained without the mirror.

#### **Data processing**

Kinematics measurements were performed from horizontal transections (top-down view). A custom program in MATLAB R2020a was used to automatically identify the outline of the fish from the raw image sequences based on the difference in contrast at the animal-fluid interface and to extract the body's centerline. The same method was used to extract the outlines of the cross-section of the tail illuminated by the laser sheet in vertical planar transections. Tail-beat amplitude (normalized to BL) and frequency  $(s^{-1})$  were measured at the tail's distal end and were averaged over three complete beat cycles for each individual. The amplitude envelopes of the fish were calculated from stacked centerlines over one complete tail beat. Tail angle was measured in degrees as the angle formed between the axis oriented in the swimming direction and the line passing through the caudal fin tip and the tail section directly posterior to the caudal peduncle. Measurements of the subtle axial displacement of the fish during a complete tail beat (surge displacement) were performed for each frame using a custom program in MATLAB R2020a that automatically tracked surface features of the fish at a location corresponding to the center of mass (COM). The instantaneous velocity of the forward and backward surges was subsequently calculated as the dividend of the linear displacement of the COM and the time increment between frames. Instantaneous acceleration was then computed as the derivative of instantaneous velocity. Surge forces were calculated as the product of the mass of the fish and instantaneous surge acceleration. Surge forces were used to determine when the body and tail achieved peak thrust throughout a complete tail beat. Note that because the fish were swimming against a steady flow, net thrust averaged zero over a complete cycle.

Fluid velocity vectors were calculated from sequential images analyzed using the DaVis 8.3 software package (LaVision, Göttingen, Germany). Only the sequences during which the fish swam within the center of the flume were considered for analysis. For horizontal and vertical planar transections, image pairs were analyzed with three passes of overlapping interrogation windows (75%) of decreasing size of 96×96 pixels to 64×64 pixels, yielding 128×128 vectors per frame. No smoothing of the velocity data was performed, but denoising was carried out using an average vector from NAN neighborhood in a 3×3 grid. Velocity data and outlines of the fishes' bodies (horizontal transection) or tail cross-section (vertical transection) were input to the Queen 2.0 pressure package for MATLAB to compute the corresponding pressure fields (code availability: http://dabirilab.com/software). Because this algorithm is sensitive to integration domain size, we selected videos where the fish maintained clearance between the walls of the flume and the tail tips approximately equal to the height of the tail (the tail occupied about 1/3 of the height of the field of view). 3D bodies inherently create 3D flows. These flows include tip vortices and may not be captured with 2D quantification techniques. Nonetheless, the evaluation and validation of this method against experimental and computational data found that this 2D approach accurately estimates the shape, timing and magnitude of pressure fields around fish-like swimmers (Dabiri et al., 2014). As such, it is appropriate for studying fish locomotion (Du Clos et al., 2019; Gemmell et al., 2015; Gemmell et al., 2016; Lucas et al., 2017; Lucas et al., 2020).

For vertical transections of the tail, pressure gradients were calculated as the pressure difference between the floward (facing lateral flow) and lee (opposite to lateral flow) surfaces of the tail. Pressures were measured along the boundary drawn around the tail cross-section illuminated by the laser sheet. The superior and inferior extremities of the profile marked the limit between the left and right sides of the tail. Although pressures differed on the floward and lee sides of the tail, the magnitude of the spanwise pressure difference was relatively uniform, similar to simulations of pressure fields along various fish tails (Song et al., 2021). Pressure fields were relative to ambient pressure, with sub-ambient and above-ambient pressures being negative and positive, respectively. The resulting force was calculated for both tail geometries by multiplying the surface area of the fins with the magnitude of the pressure gradient and the unit vector normal to the tail. The peak net thrust was calculated during maximum surge as the axial component of the normal force generated by the pressure gradient across the tail. The pressure and thrust coefficients were calculated following the methods of Lucas et al. (2020) (see Supplementary Materials and Methods, 'Calculation of the coefficient of pressure and thrust').

We estimated the forces acting on the fish's body for horizontal transections using the procedure detailed in Lucas et al. (2017). In brief, force magnitude was calculated per unit depth (because PIV data were 2D) as the product of pressure, the length of each segment between points in a calculation boundary drawn around the fish, the unit vector normal to each segment, and the corresponding body depth, giving units of Newtons (see Supplementary Materials and Methods). The vector assigned to an individual segment indicates gross thrust or drag depending on whether it is oriented in the swimming direction or posteriorly (see Supplementary Materials and Methods). Previous work indicates that when pressure effects dominate shear effects, such as in fish-like swimmers, this approach is robust to out-of-plane flows and allows for accurate estimation of forces (Lucas et al., 2017, 2020). Because the lateral component of these forces is normal to the direction of swimming and does not contribute to either thrust or drag, we only computed the axial (in the swimming direction) component to estimate thrust and drag (Du Clos et al., 2019; Gemmell et al., 2016). Here, thrust forces are positive, and drag forces are negative. The net thrust produced by the body of both species was computed for a full tail beat as the total sum of the force vectors assigned to body segments between 0.5 BL (midbody) and 0.8 BL (caudal peduncle), where most of the difference in body wave amplitude between mojarras and pinfish was observed.

#### **Statistics**

All statistical tests were performed using MATLAB R2020a. Because in most cases normality was not achieved (tested using the Kolmogorov–Smirnov test), the non-parametric Mann–Whitney U-test was used to compare means between the two fish species for fin and body geometry properties and kinematics parameters. U-Tests were also performed to compare peak pressure gradients and forces at the tail between the two fish species and to compare the net thrust produced by their body. Differences were considered significant at P<0.05. Parameters are reported as means $\pm$ s.d.

#### **RESULTS**

#### Geometry of the tails

Mojarras and pinfish are two carangiform fish species that display similar body morphologies, fin arrangements and modes of locomotion during cruising. The two species exhibited comparable morphometrics (Table 1), including similar body aspect ratios (Fig. 1; *U*-test, *P*=0.531). Mojarras possess a homocercal forked tail with two distinct, flexible fin lobes of the same size separated by a large 'notch.' In contrast, pinfish exhibit a truncate tail that is only slightly emarginated (concave trailing edge, TE; Fig. 1). Flow visualization did not reveal the presence of identifiable flow structures associated with this feature. The aspect ratio was calculated to evaluate the geometrical differences between the two tail morphologies (Fig. 1, Table 1). Although the span of the two caudal fin types was comparable (mojarra: n=12 fish, pinfish: n=10fish, U-test, P=0.621: Table 1), the 11% smaller surface area of the mojarra's tail caused by the interlobar notch was sufficient to produce a geometry with an aspect ratio of 3.25±0.20 while the flat tail of the pinfish had a statistically lower average aspect ratio of  $2.74\pm0.17$  (*U*-test, *P*<0.001; Table 1). The presence of a notch in the forked tail of mojarras was the only significant morphological difference as no other aspect of their geometry differed. For instance, the angle formed by the superior and inferior leading edges (LE) of the tails (i.e. the sweep angle) were similar (U-test, P=0.121). Additionally, the fish had comparable body aspect ratios (*U*-test, P=0.531). Therefore, any differences in the flow around the tail are expected to be only the result of the tail kinematics and/or the shape of the TE (forked versus truncate).

### Effects of tail shape on flow

During swimming trials at a cruising speed of 1.5 BL s<sup>-1</sup>, the surfaces of the forked and truncate tails were subject to some deformation. The truncate tail and each lobe of the forked tail bent along the vertical plane. This cupping pattern was caused by the superior and inferior edges of these structures leading the tail beat while their center was lagging (Fig. 2). In the forked tail, this corresponded to both the LE and TE of the fin leading the movement (Fig. 2B). This pattern was maintained across multiple steady swimming speeds (Fig. S3). In the truncate tail, only the LE were leading (Fig. 2C). Time series of the motion of the tails indicated that this cup-like shape was generally symmetrical about the midline of the fish and showed negligible variation between the two phases of a complete tail beat. In the forked tail, the two lobes showed identical patterns.

The lateral motion of both tails generated two counter-rotating vortices along the LE of the fin (Fig. 2C,F). However, where the truncate tail produced only two leading-edge vortices (LEV) along the vertical plane, the forked tail produced a total of four vortices: the same two LEV along the LE and two additional trailing-edge vortices (TEV) created by the edges of the interlobar notch (Fig. 2C). The TEV were similar in size and magnitude to the

Table 1. Fin and body geometry properties

Parameters	Mojarra	Pinfish	P-value
Fish standard length (m)	0.096±0.07	0.097±0.07	0.623
Tail surface area (cm <sup>2</sup> )	2.68±0.30	3.00±0.35	0.044
Tail aspect ratio	3.25±0.20	2.74±0.17	< 0.001
Leading edge sweep angle (deg)	67.83±5.10	70.50±4.86	0.121
Body aspect ratio	0.37±0.03	0.38±0.02	0.531

Data are means±s.d. for mojarras (*n*=12 fish) and pinfish (*n*=10 fish). *P*-values are from Mann–Whitney *U*-tests.

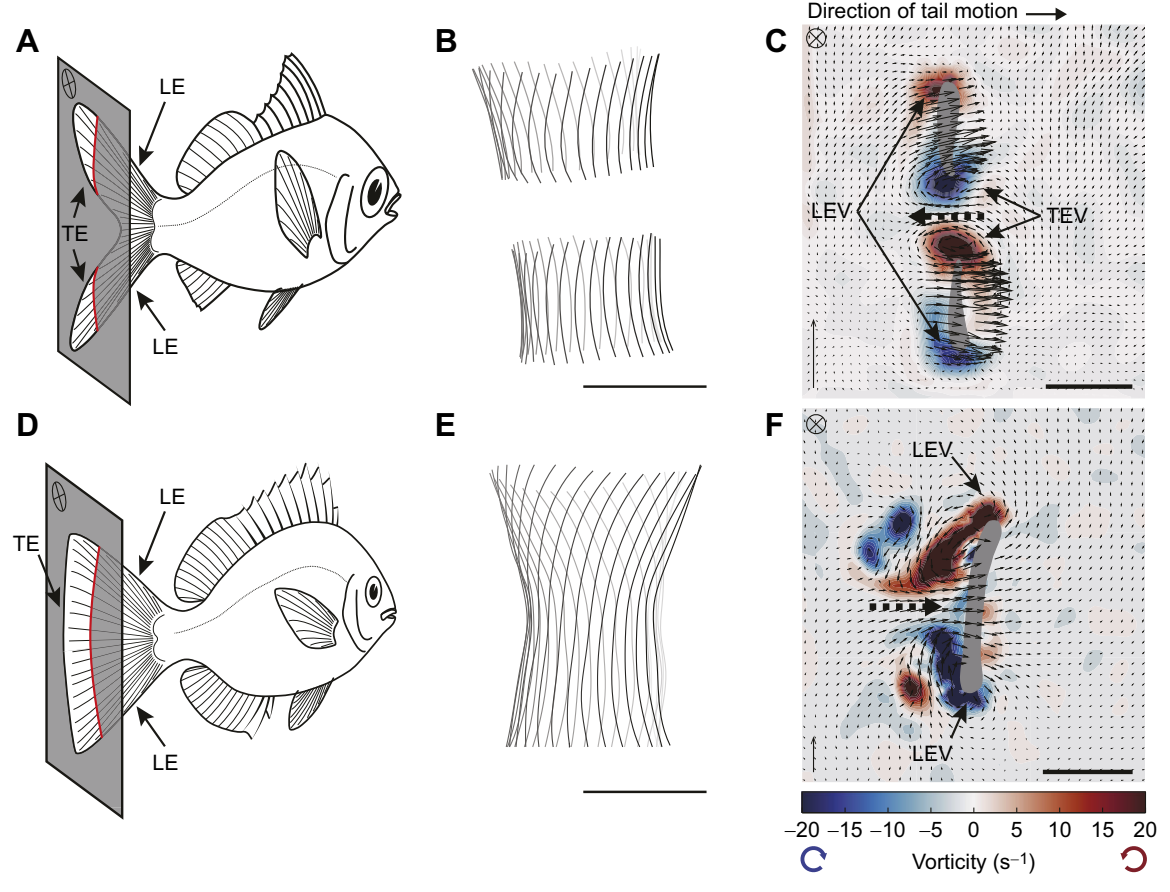


Fig. 2. Deformation and hydrodynamics of the forked tail of mojarras and the truncate tail of pinfish. (A,D) Schematic diagram of a mojarra (A) and pinfish (D) illustrating the planes used to perform vertical transections of the flow around the tail. Fluid flows were visualized from the posterior view (indicated by the cross in the top left corner of the plane). The leading edges (LE) and trailing edges (TE) were identified for both tails. (B,E) Stacked vertical transections of the tail of mojarras (B) and pinfish (E) illustrating the cupping of the fin's surface during a complete tail beat (from light to dark hues in 0.01 s increments). Note the gap between the lobes of the caudal fin of mojarras. (C) The lateral displacement of the forked tail of mojarras generates four distinct vortices – two leading-edge vortices (LEV) and two trailing-edge vortices (TEV). (F) Pinfish only generate two LEV. Note that the single trailing edge is out of plane. The thick dashed black arrows indicate the direction of the jet of water produced during the motion of the tails toward the right of frames in C and F. All scale bars: 1 cm; black vertical scale arrows: flow of 20 cm s<sup>-1</sup>.

leading LEV. The LEV and TEV forming along the fin's edges persisted throughout the majority of a tail beat cycle, though they reversed sign upon the change in direction of the tail. Another notable difference between the two tail morphologies is the direction of the flow orthogonal to the tail induced by the formation of LEV and TEV. The LEV produced by the truncate tail were funneled inward, entraining water toward the tail (Fig. 2F). This caused an increase in fluid velocity between the vortices. In contrast, the LEV of the forked tail did not generate a comparable spanwise increase in fluid velocity. Rather, inward flow was produced along individual fin lobes through the action of one LEV and one TEV essentially acting collectively like the two LEV of the truncate tail (Fig. 2C). Because the interlobar notch formed counterrotating TEV, water was entrained with increased velocity between the lobes in the opposite direction to the movement of the tail (also opposite to that of the inward flow generated by the truncate tail). Contrary to the case for the truncate tail, this jet of water was not directed at the tail surface.

#### Roles of the fin and body in swimming forces

Oscillations of the tail led to variation in instantaneous net thrust throughout a tail beat cycle. The best indicators of peak thrust production during swimming were the subtle surges of the body (forward displacement of the center of mass) during cruising (Figs 3 and 4). By definition, during steady swimming, the axial acceleration of the center of mass of the fish is zero. Thus, positive surges indicate net forward accelerations equating to excess thrust, whereby propulsive forces generated by the tail (and body) periodically exceed drag. Conversely, negative values are associated with phases when drag forces dominate and slightly decelerate the fish. For instance, this occurs when the tail is parallel to the direction of swimming and thus generates no axial forces. The frequency of these thrust and drag cycles was twice that of the motions of the tail over one complete tail beat (Fig. S4). Both fishes produced surge thrust with comparable magnitudes (U-test, P=0.653), averaging 0.79±0.41 and 0.91±0.50 mN for mojarras (n=5 fish) and pinfish (n=5 fish), respectively.

Tail kinematics were generally the same and corresponded similarly to phases of thrust production (Figs 3 and 4, Table 2). In both cases, the magnitude of surge thrust increased from 0 as the caudal fin accelerated from its most lateral position toward the midline, and remained positive (thrust phase) until the tail reached mid-stroke and peak lateral velocity (Figs 3 and 4). This positive surge phase corresponded to peak pressure gradients across the tail. However, the pressure magnitudes differed significantly, with 12.84±1.86 and 19.82±2.77 Pa (*U*-test, *P*<0.001) for the forked and

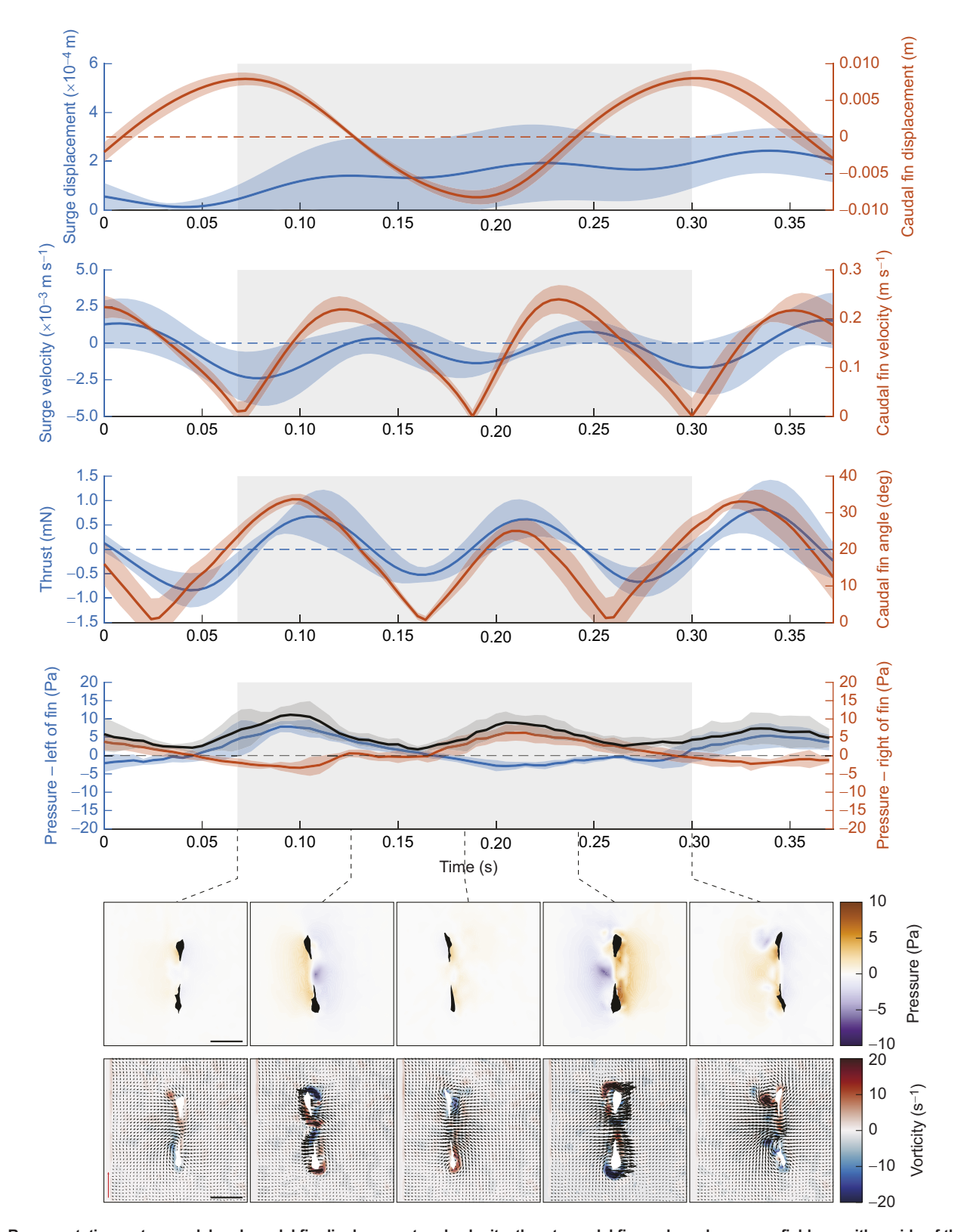


Fig. 3. Representative rostro-caudal and caudal fin displacement and velocity, thrust, caudal fin angle and pressure fields on either side of the caudal fin of mojarra swimming at 1.5 BL s<sup>-1</sup>. The fish swam against a steady flow, so net thrust averages zero over a complete tail-beat cycle. The black pressure trace represents the pressure gradient across the caudal fin. The gray rectangle indicates one complete tail beat. The time series of pressure and vorticity fields from vertical planar transections of the tail (posterior view) are for the same tail beat. Colored lines and shading indicate means and s.d. Scale bars: 1 cm; red vertical scale arrow: flow of 20 cm s<sup>-1</sup>. BL, body lengths.

the truncate tails, respectively (Figs 3, 4 and 5A). The magnitude of the positive pressure fields generated by the forked tail was 25.2% less than that of the truncate tail on average (Fig. S4; *U*-test,

P=0.005), and the sub-ambient pressure fields on the opposite side of the lobes were 48.7% weaker (Fig. S4; U-test, P<0.001). Because of these differences and given the smaller surface area of the forked

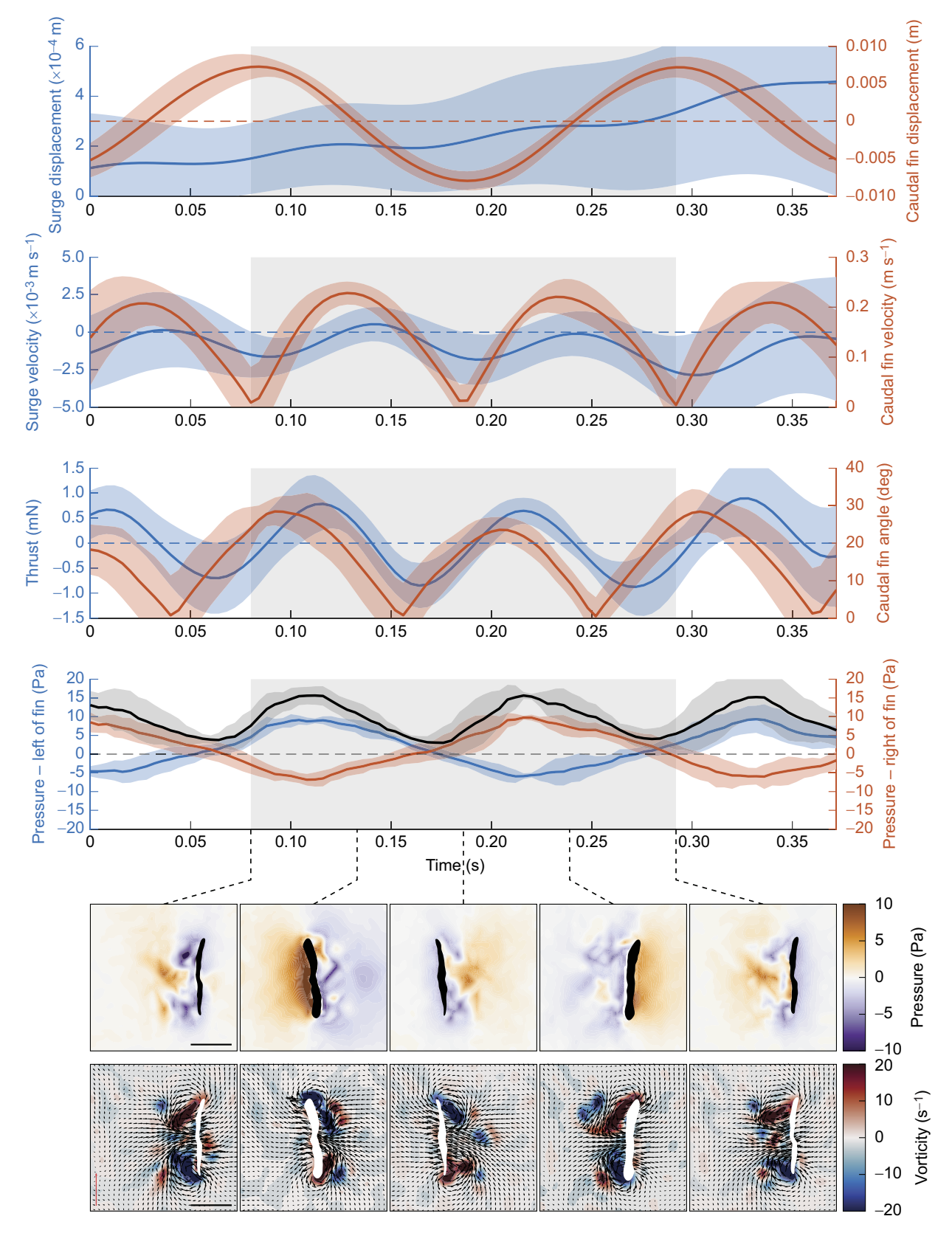


Fig. 4. Representative rostro-caudal and caudal fin displacement and velocity, thrust, caudal fin angle and pressure fields on either side of the caudal fin of pinfish swimming at 1.5 BL s<sup>-1</sup>. The fish swam against a steady flow, so net thrust averages zero over a complete tail-beat cycle. The black pressure trace represents the pressure gradient across the caudal fin. The gray rectangle indicates once complete tail beat. The time series of pressure and vorticity fields from vertical planar transections of the tail (posterior view) are for the same tail beat. Colored lines and shading indicate means and s.d. Scale bars: 1 cm; red vertical scale arrow: flow of 20 cm s<sup>-1</sup>.

Table 2. Kinematics parameters

Parameters	Mojarra	Pinfish	P-value
Tail-beat frequency (s <sup>-1</sup> )	4.86±0.71	4.76±0.78	0.571
Tail-beat amplitude (BL)	0.16±0.03	0.15±0.02	0.740
Maximum angle of attack (deg)	31.4±4.6	27.3±4.9	0.038
Peak surge thrust (mN)	0.79±0.41	0.91±0.50	0.653
Re	13,615±1896	13,929±2024	0.623
St	0.49±0.04	0.45±0.06	0.161

Data are means±s.d. of mojarras and pinfish swimming steadily at a prescribed speed of 1.5 BL s<sup>-1</sup>. *P*-values are from Mann–Whitney *U*-tests. BL, body lengths; *Re*, Reynolds number; *St*, Strouhal number.

tail, this resulted in 39.3% weaker forces acting upon its surface compared with the truncate tail (*U*-test, *P*<0.001). However, because of the steeper angle of the forked tail relative to the direction of swimming during this phase (Figs 3 and 4, Table 2), the resulting thrust component at the tail was oriented more medially. It was only 18.6% weaker (Fig. 5C; U-test, P<0.001). Peak thrust was achieved in the forked fin when the angle of attack reached 29.7±4.4 deg. This was significantly more than the truncate caudal fin, whose angle of attack was  $23.9\pm4.8$  deg (*U*-test, *P*=0.038). Despite this improvement, the coefficient of pressure  $(C_P)$  and thrust  $(C_F)$  remained significantly less for the forked tail (Fig. 5B,D; Utest, P < 0.001), indicating lower overall efficiency. After passing the midline, surge thrust became negative as the lateral velocity of the tail and the magnitude of the pressure gradients decreased gradually. This indicated that drag forces acting on the body counteracted the forces produced by the tail. The drag phase persisted until the caudal fin reversed direction (Figs 3 and 4).

Tail-beat amplitude was similar between the two tail types (Table 2; *U*-test, *P*=0.740). However, time series of the centerlines of the two fish species showed that mojarras recruited the body section anterior to the tail (from 0.5 to 0.8 BL) significantly more than pinfish (Fig. 6). For instance, the amplitude of the body waves

propagating through this section of the body, in particular the caudal peduncle, was twice that of pinfish (Fig. 6C; *U*-test, P<0.001). To understand the differences between the two swimmers, it is essential to compare the thrust produced by the body, not just the tail. Estimations of thrust and drag forces along this body section indicate that mojarras (n=10 fish) produced up to  $15.0\pm9.3$  mN of net thrust with their body during a full tail beat, while pinfish (n=7 fish) generated only net drag of  $-1.3\pm4.2$  mN (U-test, P<0.001; Fig. 6D). While this is equivalent to 56.8% of the total gross thrust produced by mojarras during a full tail beat, pinfish produced nearly as much drag as thrust, thus resulting in no net thrust produced by the body.

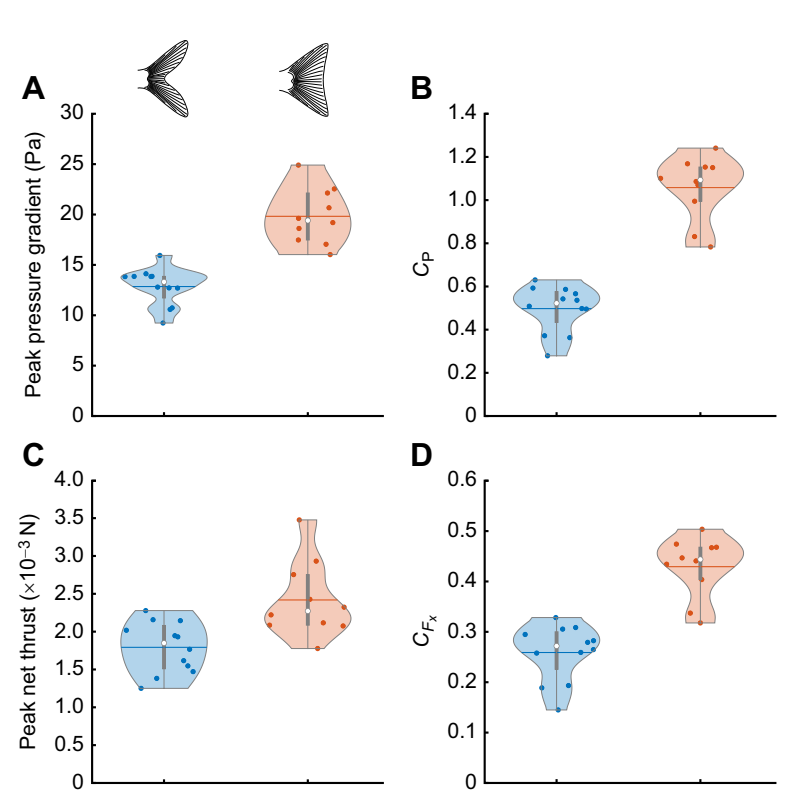
#### **Energetics of differing tail shapes during cruising**

The COT of mojarras and pinfish followed a J-shaped trend, commonly reported in other species (Korsmeyer et al., 2002; Webb, 1975). Mojarras and pinfish reached their optimal swimming speed, the speed at which the net energetic cost of swimming is minimal, at  $U=1.21~\rm BL~s^{-1}$  and  $U=1.99~\rm BL~s^{-1}$ , respectively. The net COT at  $1.5~\rm BL~s^{-1}$  was  $3.831\pm1.543$  and  $1.789\pm0.683~\rm J~m^{-1}~kg^{-1}$  for mojarras and pinfish, respectively (U-test, P=0.032). Throughout the entire range of swimming speeds tested, the mojarras exhibited a higher COT (Fig. 7).

#### **DISCUSSION**

#### **Drag-based propulsion in forked fin**

The tail morphology of fishes plays an integral role in swimming performance because it regulates the nature and magnitude of the forces produced during undulatory swimming (Blake, 2004; Fletcher et al., 2014; Lauder, 2000). Syntheses of undulatory fish locomotion explain that truncate tails are better suited for fast accelerations powered by acceleration reaction forces, while forked tails promote economical, fast cruising via lift-based thrust (Helfman et al., 2009; Lauder, 2000; Sfakiotakis et al., 1999).



Mojarra

Pinfish

Pinfish

Mojarra

Fig. 5. Peak pressure gradients and thrust generated by the forked and truncate tails. (A) Peak pressure gradient forming across the tail during maximum surge (U-test, P<0.001). (B) Coefficient of pressure ( $C_p$ ; U-test, P<0.001). (C) Peak net thrust component calculated from the force normal to the tail during maximum surge (U-test, P=0.004). (D) Coefficient of thrust of the two tails ( $C_{F_x}$ ; U-test, P<0.001). The white dot in the violin plots indicates the mean, and the horizontal line is the median. Shading represents the kernel density estimate for the data.

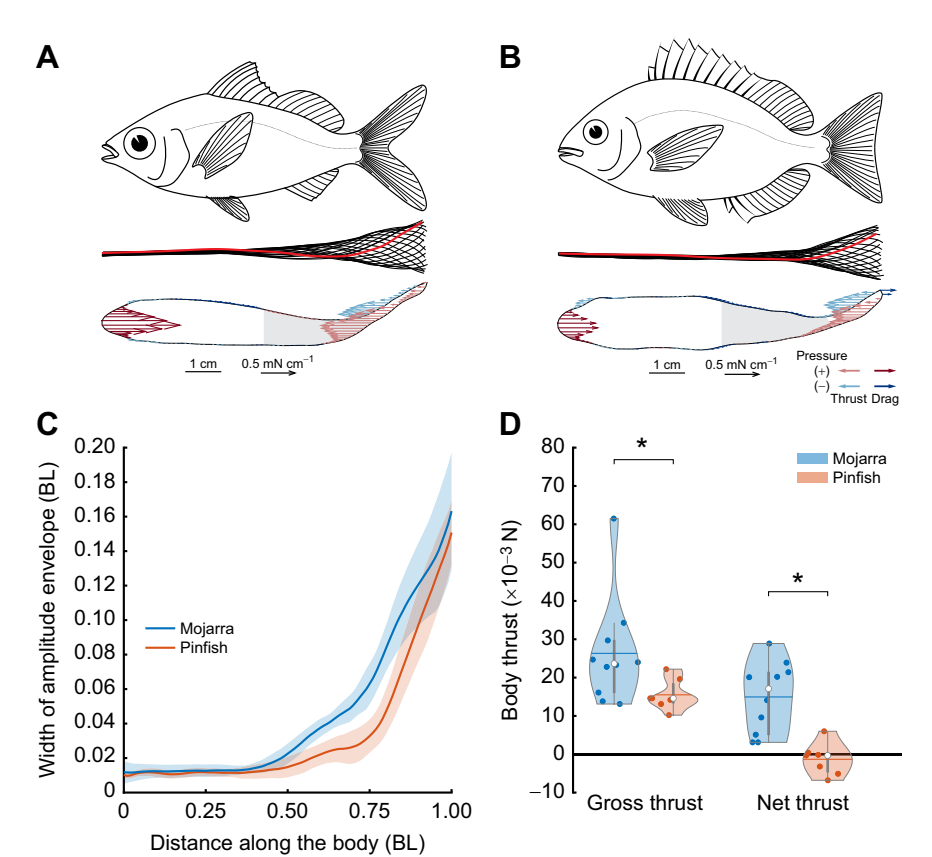
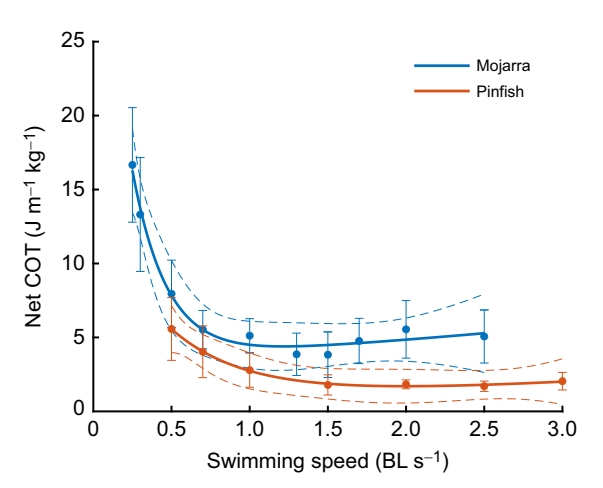


Fig. 6. Body wave amplitude and resulting forces in mojarra and pinfish swimming at 1.5 BL s<sup>-1</sup>. Line art for one representative mojarra (A) and pinfish (B) showing lateral view (top), stacked centerlines (middle) and dorsal view with forces acting on the body (bottom). The last of these corresponds to the realization highlighted in red in the stacked centerlines. (C) Mojarras display wider body wave amplitude than pinfish along the section of the body anterior to the tail from 0.5 to 0.8 BL (gray shaded area in top-view force profiles in A and B). Colored lines and shading indicate means and s.d. (D) The mojarra body generated more thrust than the pinfish body over a full tail beat. Asterisks indicate statistical significance between pairs for gross thrust (*U*-test, P=0.027) and net thrust (*U*-test. P<0.001). The white dot in the violin plots indicates the mean, and the horizontal line is the median. Shading represents the kernel density estimate for the data.

Unlike most virtual and mechanical models studied to date, the high aspect ratio tail found in many numerically dominant fish families is a pliable feature whose constituent fin rays can modulate the shape (Esposito et al., 2012; Lauder, 2000; Standen and Lauder, 2005). Our results show that flexibility enables the cupping of each fin lobe during lateral motions of the tail (Figs 2 and 8; Fig. S4). This type of deformation has not been reported in forked tails previously. Studies



**Fig. 7. Net cost of transport.** Mojarras (n=5 fish) and pinfish (n=5 fish) reached their lowest cost of transport (COT) at U=1.21 BL s $^{-1}$  and U=1.99 BL s $^{-1}$ , respectively. The equation for the fitted lines is COT= $\alpha$ e $^{\beta U}$ + $\gamma$ e $^{8 U}$ , where  $\alpha$ =39.43 J m $^{-1}$  kg $^{-1}$ ,  $\beta$ =-4.52 s BL $^{-1}$ ,  $\gamma$ =3.43 J m $^{-1}$  kg $^{-1}$ ,  $\delta$ =0.17 s BL $^{-1}$  ( $R^2$ =0.79) for mojarra and  $\alpha$ =13.07 J m $^{-1}$  kg $^{-1}$ ,  $\delta$ =-2.10 s BL $^{-1}$ ,  $\gamma$ =0.87 J m $^{-1}$  kg $^{-1}$ ,  $\delta$ =0.28 s BL $^{-1}$  ( $R^2$ =0.62) for pinfish. Error bars indicate standard deviation and dashed lines represent 95% confidence interval.

of oscillating flexible fin analogs showed that one advantage of cupping is the production of about 25% more thrust than a flat rigid fin (Feilich and Lauder, 2015; Tangorra et al., 2009). The bending of high aspect ratio tails over their entire span has been the subject of recent studies (Bergmann et al., 2014; Lucas et al., 2014; Rosic et al., 2017). Nevertheless, forked caudal fins are typically described as undeformable tapered hydrofoils (see Fig. 8) (Sfakiotakis et al., 1999; Wainwright and Lauder, 2020; Zhu et al., 2019). No data currently exist to compare the performance of cupping versus rigid hydrofoil-shaped fins. We identified several key differences in the conformation and hydrodynamics between the flexible forked tail of mojarras and lunate tails. These address possible limitations of generalizing caudal fin shapes. Because of the cupping of the fin lobes of the flexible forked tail, both the LE and TE are leading lateral tail excursions during a tail beat (Figs 2B and 8; see Supplementary Materials and Methods). In contrast, the pitching and heaving motions of rigid high aspect ratio tails causes the LE to be leading during lateral excursions, while the TE formed by the fork are lagging (Chopra, 1974; Sfakiotakis et al., 1999; Wainwright and Lauder, 2020). Numerical and experimental studies show that the oscillating motion and hydrofoil geometry of such tails collectively generate lift forces through a LE suction mechanism (Borazjani and Daghooghi, 2013; Song et al., 2021; Zhu et al., 2019). Pressure along the surface of the fin decreases substantially as a result of the single LEV forming when water travels around the rounded LE (Borazjani and Daghooghi, 2013; Wang et al., 2019b). Our findings indicate the presence of not one but two edge vortices along the LE and TE of the forked tail.

Considered separately, each fin lobe of the mojarra's tail acts similarly to the truncate tail of pinfish both mechanically and hydrodynamically. Because the truncate fin of pinfish is flexible, lateral oscillations during steady swimming cause a spanwise

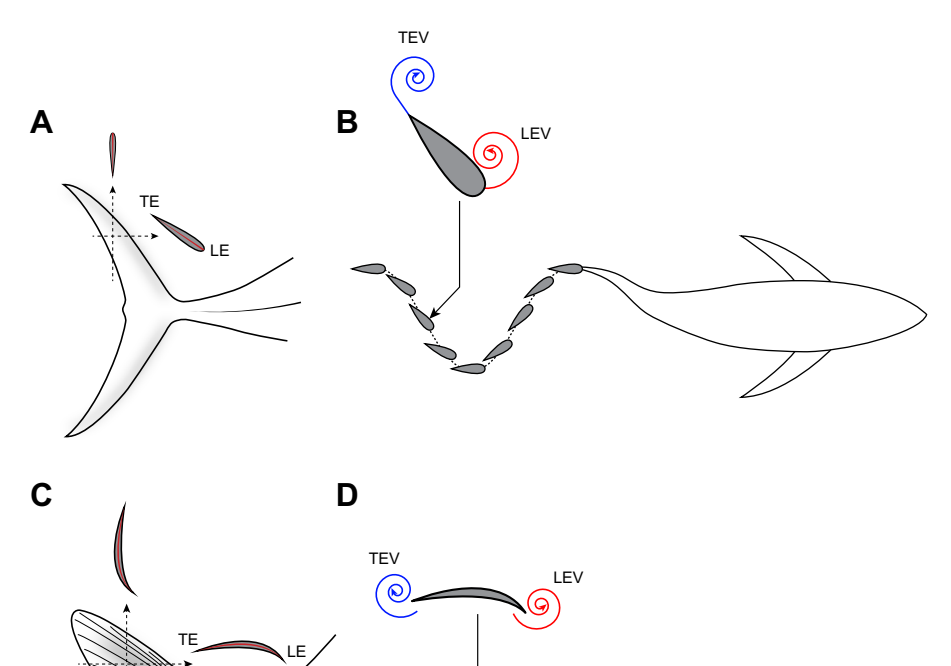


Fig. 8. Conceptual diagram of tail conformations for a lunate tail and the flexible forked tail of mojarras. (A,C) Lateral views of the lunate tail of tunas (A) and the flexible tail of mojarras (C) showing the vertical and horizontal profiles of the superior lobe. Red lines across profiles in A and C represent the center of the chord of the profiles to emphasize their shape: straight chord for the lunate tail and cupped chord for the flexible forked tail. (B,D) Trails of the lunate tail (B; adapted from Sfakiotakis et al., 1999) and the tail of mojarras (D) showing the change in the angle of attack over time and change in fin surface conformation. The LEV and TEV are shown through vorticity.

deformation of its surface (Fig. 2), similar to the cupping of the forked fin lobes and the well-studied cupping pattern of the broad tail of bluegill sunfish (Lauder, 2000; Lauder and Drucker, 2002; Tytell, 2006). Because of the geometry of the truncate tail, only two vortices formed along the LE. Experimentally derived pressure fields showed an increase in the magnitude of the positive and negative pressures along the floward (within the cup) and lee (opposite side) surfaces, respectively, during tail displacement (Fig. 4). However, positive pressures contributed more to the resulting pressure gradient across the tail (U-test, P<0.001). Because we only investigated one plane across the tail, we could not capture the potential effects on pressure near the tip of the tail from vortex shedding. Nonetheless, our findings are in agreement with computational models of non-forked tails (Song et al., 2021) and demonstrate the acceleration reaction-based (push) rather than liftbased (suction) properties of the truncate morphology. Similar to this study, these models also found that comparably weaker positive pressure fields formed along the stoss surface of a higher aspect ratio tail (Fig. 3; Fig. S4). However, they and others (van Buren et al., 2017) show that higher aspect ratio geometries produce negative pressures of greater magnitude than a truncate morphology. This difference is explained by their use of the traditional hydrofoil profile of lunate tails that induces conditions favorable for the production of strong leading-edge suction through a unique LEV. In this case, the individual curved lobes of the forked tail produce two edge vortices like that of the truncate tail. These similar flow conditions result in pressure gradients across the tail where the magnitude of positive pressures is proportionally greater than the negative pressures. The pressure difference across the tail contributes to the manifestation of propulsion (Dubois et al., 1978; Lucas et al., 2020; Song et al., 2021). Our findings indicate

that the flexible forked tail of mojarras operates via the same fundamental drag-based propulsive mechanism of the truncate tail during continuous swimming. Here, we provide evidence that challenges the established notion that high aspect ratio caudal fins exploit only lift-based forces at cruising speeds (Helfman et al., 2009; Sfakiotakis et al., 1999).

#### A forked tail does not always provide a cruising advantage

Changes in the kinematics of the tail, such as frequency and amplitude, can explain differences in the forces experienced by this propulsor during swimming (Bainbridge, 1958; Chopra, 1976; Saadat et al., 2017). Here, this was not the case as we found that despite contrasting tail morphologies, these kinematics parameters were similar (Table 2). Instead, propulsive forces were modulated by altering the angle of the tail relative to the flow and by regulating the amplitude of body undulations anterior to the tail. From experimentally derived pressure fields, we found that the reduced surface area of the forked caudal fin generated 31% weaker pressure gradients (Figs 3, 4 and 5; Fig. S4). Assuming a uniform distribution of the pressure gradients over the entire surface of both caudal fins, the forked fin cannot produce the same force as the truncate tail given the observed kinematics. Here, the forked tail produced only 3/5 of the forces generated by the truncate tail. However, the thrust component of the normal force acting on the fin's surface depends on the angle of the propulsor relative to the swimming direction (Helfman et al., 2009; Webb, 1978a). Self-propelled mechanical analogs indicate that the angle of attack of the caudal fin can be changed by modulating the kinematics of the section of the body anterior to the tail to achieve comparable propulsive outputs with differing tail morphologies (Feilich and Lauder, 2015; Krishnadas et al., 2018). By increasing the lateral displacement of the caudal

peduncle, mojarras also increase the angle of attack of their tail during the thrust phase of a tail beat, thus orienting the thrust component more axially. In doing so, the 40% difference in the strength of the forces produced at the tail is brought to only a 18.6% difference in net thrust compared with the truncate tail (Fig. 5). However, the strong stagnation effect along the floward surface of the truncate tail under high pressure (Fig. 4) and its overall larger surface area were previously shown to increase pressure compared with higher aspect ratio tails (Song et al., 2021). Despite a net improvement in thrust production, the coefficient of pressure  $(C_P)$ and thrust  $(C_{F_x})$  remained significantly less for the forked tail (Fig. 5; *U*-test, *P*<0.001), indicating lower overall efficiency. Despite the proportionally greater contribution of these forces to thrust in the forked tail, there still exists a deficit in the net thrust produced relative to the truncate tail due to the reduced surface area of the forked tail. The magnitude of the forces generated by propulsive structures during swimming is dependent in part on the shape and drag characteristics of the swimmer (Dubois et al., 1978; Maertens et al., 2015; Saadat et al., 2017). Given the similar body length, shape and mass of mojarras and pinfish, a very similar amount of net thrust must be produced to maintain the same cruising speed. How can the mojarra create similar total net thrust when it produces less force than pinfish with its tail?

By focusing on the caudal fin only, one cannot capture the full extent of the propulsive mechanisms employed by the fish during sustained body/caudal fin undulatory swimming. Time series of the fish's centerline showed that mojarras recruited significantly more body bending along the body section extending from the caudal peduncle to the midbody (Fig. 6; *U*-test, *P*<0.001). Previous studies on carangiform swimmers posited that body undulations could generate thrust from the positive and negative pressure areas resulting from the lateral displacement of the body anterior to the tail (Dubois et al., 1974; Lucas et al., 2020; Müller et al., 1997; Tytell, 2007). Producing body waves 1.8 times wider than those of pinfish enables mojarras to generate a significant amount of net thrust over a full tail beat with their body while pinfish produce only net drag. As such, mojarras can compensate for comparatively less thrust produced at the tail (Fig. 6). Previous studies on lamprey (Gemmell et al., 2016) and trout (Lucas et al., 2020) showed comparable benefits in increasing upstream body bending to produce more thrust and maintain greater swimming speeds.

However, involving more of the body to compensate for the thrust deficit of the forked tail could incur an additional energetic cost at cruising speeds due to increased acceleration reaction forces caused by wider lateral excursions into the flow (Maertens et al., 2015; Webb, 1992). Increased recruitment of the anterior axial musculature during undulatory swimming increases power consumption to offset the increase in fluid forces (Korsmeyer et al., 2002; Videler and Weihs, 1982). We found that the net COT of mojarras was 2.1 times higher than that of pinfish on average to maintain the same relative swimming speeds (Fig. 7). In sum, these findings demonstrate that a forked tail design is not always advantageous at cruising speeds. Contrary to our current knowledge of fish propulsion, the mojarra's flexible forked caudal fin shows deficiencies in its ability to generate enough thrust compared with a truncate tail. The lower performance of this morphology is reflected in the higher energetic demand imposed by the recruitment of more of the axial musculature.

#### Functional significance of contrasting tail morphologies

We did not find evidence that the flexible forked tail of mojarras employed the lift-based propulsive mechanism observed in hydrofoil-shaped lunate tails during cruising. Instead, the cupping of individual fin lobes produces edge vortices like that of the truncate tail, resulting in pressure gradients where the magnitude of positive pressures is proportionally greater than that of negative pressures. This drag-based fin conformation persisted below and above their optimal swimming speeds (Fig. S4). Contrary to the existing paradigm of forked tail functionality, we found that this flexible tail design did not confer an energetic and propulsive advantage during cruising. In fact, the truncate tail of pinfish outperformed it. Yet, many successful and abundant families such as Carangidae (e.g. pompano, trevally, jack), Clupeidae (e.g. herring, sardine) and Engraulidae (e.g. anchovy) feature such flexible fin morphology. This raises the question: if a flexible forked tail does not confer an efficiency advantage for cruising, can it provide other functional benefits?

We compared these two tail types with the common assumption that the evolution of form and function is driven primarily by efficiency. However, certain behaviors may be driven by a need to supply additional mechanical power rather than to minimize swimming costs (Kendall et al., 2007). While a flexible forked tail seemingly appears less favorable for cruising, it may constitute a tradeoff between form and function in various contexts. Body structures develop according to their importance for primary living functions (Russo et al., 2007; Sagnes et al., 1997; Stoner and Livingston, 1984). Therefore, it is also important to consider how functional rather than purely structural attributes may be advantageous for feeding, escape, schooling, stability in turbulence, and migrations. Previous studies proposed the interlobar notch of forked caudal fins to reduce drag from the body wake, thus limiting the energy demand during swimming (Fletcher et al., 2014; Helfman et al., 2009; Lauder, 2000). Under this assumption, the COT of mojarras should be less than that of pinfish; however, our data do not support this. Another proposed functional benefit of forked caudal fins comes from the observation that the wake of schooling fish can energize the flow over the tail of downstream individuals, thus contributing to greater lift forces and improved performance (Li et al., 2020; Liao, 2022). Neither of the two species used in this study exhibit schooling behavior, and in fact they are known to be territorial (Eschmeyer and Herald, 1999; Nelson, 2002). There are, however, many species with forked tails that do exhibit schooling, and most are planktivores like mojarras. Adult Carangidae that feed on larger prey (e.g. other fishes) display a more rigid, lunate-like forked tail, but the planktivorous juveniles exhibit a flexible forked tail comparable to that of mojarras. This correlation between planktivory and a flexible forked tail suggests this morphology may provide an advantage during foraging that would suggest planktivory as a driver of the development of a flexible forked tail.

In many fishes, the caudal fin is used not exclusively for forward propulsion but also to generate forces that play a key function in maneuvering and body stabilization in the water column (Lauder, 1989; Lauder and Drucker, 2004; Videler, 1977; Weihs, 1973a). Early studies of the musculoskeletal structures of flexible forked tails like that of mojarras suggest that the conformation of each lobe can be actively modulated separately to aid in control of orientation and body position (Flammang and Lauder, 2009; Lauder, 1982, 1989). While a full analysis of tail lobe motions and the resulting effects on maneuverability is beyond the scope of this study, we noted that the lobes were not kept at equal angles relative to the flow during occasional vertical repositioning of the fish in the swim tunnel (Fig. S5). By using each tail lobe independently, forked tails may exhibit functionality beyond simple forward propulsion.

Similar to the heterocercal tail of some sharks, they may vector water momentum in appropriate directions to control postural stability during cruising (Wilga and Lauder, 2002). Even truncate tails can generate complex conformations to perform maneuvers (Esposito et al., 2012). However, the motions of each constituent fin ray intrinsically depend on the movements of the other fin rays and on the fluid forces acting along the entire span of the tail (Esposito et al., 2012; Lauder, 1989, 2000). Thus, separately controllable fin lobes should have improved mobility and would likely promote faster, more controllable changes to body positions as a result. This may confer an advantage in flows and turbulent environments where maintaining a stable posture is needed. This could be important to planktivorous fish groups such as Carangidae, Clupeidae and Engraulidae whose acute head and body postural control is necessary to successfully identify and target small, transparent, evasive prey scattered in the water column (Hunter, 1981). In this context, a forked tail may facilitate enhanced capture success of small, evasive prey such as larvae and copepods which comprise the majority of the mojarra's diet. In contrast, L. rhomboides exhibits a more generalist diet as they demonstrate omnivory, carnivory and herbivory at different times, locations and stages of development (Stoner, 1980). They also feed heavily on benthic prey and adult pinfish also frequently consume small fishes (Carr and Adams, 1973). Thus, the need to generate high accelerations to ambush their prey is perhaps another driver behind the development of a truncate tail. Another advantage of using the tail to generate thrust and control body position is the potential for limiting the use of pectoral fins that would invariably increase induced drag and energetic costs of cruising (Webb, 2005). Thus, while not as efficient in steady, laminar flows as a truncate caudal fin, a forked (non-lunate) tail may represent a tradeoff between a low COT and enhanced stability and maneuverability that could increase prey capture success. Thus, it may not be coincidental that many successful planktivorous fishes such as herrings, sardines and anchovies possess a forked (non-lunate) tail like that of mojarras.

## **Conclusions**

The common generalization surrounding the shape of the caudal fins of fishes is that flat, truncate tails are best suited for fast accelerations, while forked tails promote economical, fast cruising (Blake, 2004; Fletcher et al., 2014; Helfman et al., 2009; Sfakiotakis et al., 1999). By comparing the energetics and hydrodynamics of two fish species displaying contrasting tail shapes, we experimentally show that a truncate tail morphology can perform better than a forked morphology during cruising. The reduced surface area of forked, non-lunate tails appears to adversely impact thrust capabilities while increasing the energetic costs at cruising speeds. We found that this reduced efficiency is associated with increased lateral body kinematics to maintain similar thrust outputs. This suggests an evolutionary tradeoff between efficiency and other ecologically important parameters, such as stability. Fishes have influenced the design of many underwater vehicles, whose development was motivated in part by the aim of improving efficiency and performance (Aubin et al., 2019; Katzschmann et al., 2018; Neveln et al., 2013; Wang et al., 2019a; White et al., 2021). However, many of these devices employ rigid flat or lunate propulsors. These design constraints may impede fine-scale adjustments of the fin's shape that modulate the magnitude and direction of propulsive forces. Our results offer insights into the benefits and tradeoffs of two typical tail morphologies within bony fishes and improve our understanding of functional and ecological

components of fish swimming that may aid the development of more capable bio-inspired underwater technologies.

#### Acknowledgements

We would like to thank Gabrielle Scrogham, Daryl Gibson and Victoria Scriven for their generous assistance with specimen collection. We also want to acknowledge the USF 3D printing service and the USF Physics Machine Shop for assistance with flume modification. We are grateful to Stephen Deban, John Dabiri and Ryan Carney for their helpful comments on the initial draft. We also thank three anonymous reviewers for their insightful comments on the manuscript.

#### Competing interests

The authors declare no competing or financial interests.

#### **Author contributions**

Conceptualization: N.B.T., B.J.G.; Methodology: N.B.T.; Software: N.B.T.; Validation: B.J.G.; Formal analysis: N.B.T.; Investigation: N.B.T., B.J.G.; Resources: B.J.G.; Data curation: N.B.T.; Writing - original draft: N.B.T.; Writing - review & editing: N.B.T., B.J.G.; Visualization: N.B.T.; Supervision: B.J.G.; Project administration: B.J.G.; Funding acquisition: B.J.G.

#### **Funding**

This project was supported by funding to B.J.G. from the National Science Foundation (CBET-FD 2100703) and the Alfred P. Sloan Foundation.

#### Data availability

The fish swimming data and metadata files reported in this investigation, as well as custom MATLAB scripts developed to compute kinematics, pressure fields and forces are available from the figshare digital repository: https://doi.org/10.6084/m9.figshare.19184633.

#### References

- Aubin, C. A., Choudhury, S., Jerch, R., Archer, L. A., Pikul, J. H. and Shepherd, R. F. (2019). Electrolytic vascular systems for energy-dense robots. *Nature* 571, 51-57. doi:10.1038/s41586-019-1313-1
- **Bainbridge, R.** (1958). The speed of swimming of fish as related to size and to the frequency and amplitude of the tail beat. *J. Exp. Biol.* **35**, 109-133. doi:10.1242/ieb.35.1.109
- Bainbridge, R. (1963). Caudal fin and body movement in the propulsion of some fish. J. Exp. Biol. 40, 23-56. doi:10.1242/jeb.40.1.23
- Bergmann, M., Iollo, A. and Mittal, R. (2014). Effect of caudal fin flexibility on the propulsive efficiency of a fish-like swimmer. *Bioinspir. Biomim.* 9, 046001. doi:10. 1088/1748-3182/9/4/046001
- **Blake, R. W.** (2004). Fish functional design and swimming performance. *J. Fish Biol.* **65**, 1193-1222. doi:10.1111/j.0022-1112.2004.00568.x
- Blank, J. M., Farwell, C. J., Morrissette, J. M., Schallert, R. J. and Block, B. A. (2007). Influence of swimming speed on metabolic rates of juvenile Pacific Bluefin Tuna and Yellowfin Tuna. *Physiol. Biochem. Zool.* **80**, 167-177. doi:10.1086/510637
- Blaxter, J. H. S. (1969). Swimming speeds of fish. FAO Fish. Rep. 62, 69.
- Borazjani, I. and Daghooghi, M. (2013). The fish tail motion forms an attached leading edge vortex. *Proc. R. Soc. B* **280**, 20122071. doi:10.1098/rspb.2012.2071
- **Borazjani, I. and Sotiropoulos, F.** (2009). Why don't mackerels swim like eels? The role of form and kinematics on the hydrodynamics of undulatory swimming. *Phys. Fluids* **21**, 091109. doi:10.1063/1.3205869
- Breder, C. M. (1926). The locomotion of fishes. Zoologica 4, 159-297. doi:10.5962/p.203769
- **Brücker, C. and Bleckmann, H.** (2010). Vortex dynamics in the wake of a mechanical fish. *Exp. Fluids* **43**, 799-810. doi:10.1007/s00348-007-0359-2
- Carr, W. E. S. and Adams, C. A. (1973). Food habits of juvenile marine fishes occupying seagrass beds in the estuarine zone near Crystal River, Florida. *T. Am. Fish Soc.* 102, 511-540. doi:10.1577/1548-8659(1973)102<511:FHOJMF>2.0. CO:2
- Chopra, M. G. (1974). Hydromechanics of lunate-tail swimming propulsion. J. Fluid Mech. 64, 375-392. doi:10.1017/S002211207400245X
- Chopra, M. G. (1976). Large amplitude lunate-tail theory of fish locomotion. J. Fluid Mech. 74, 161-182. doi:10.1017/S0022112076001742
- Dabiri, J. O., Bose, S., Gemmell, B. J., Colin, S. P. and Costello, J. H. (2014). An algorithm to estimate unsteady and quasi-steady pressure fields from velocity field measurements. J. Exp. Biol. 217, 331-336. doi:10.1242/jeb.092767
- **Dickinson, M. H.** (1996). Unsteady mechanisms of force generation in aquatic and aerial locomotion. *Am. Zool.* **36**, 537-554. doi:10.1093/icb/36.6.537
- Dickinson, M. H., Lehmann, F.-O. and Sane, S. P. (1999). Wing rotation and the aerodynamic basis of insect flight. Science 284, 1954-1960. doi:10.1126/science. 284.5422.1954

- Du Clos, K. T., Dabiri, J. O., Costello, J. H., Colin, S. P., Morgan, J. R., Fogerson, S. M. and Gemmell, B. J. (2019). Thrust generation during steady swimming and acceleration from rest in anguilliform swimmers. *J. Exp. Biol.* 222, jeb212464. doi:10.1242/jeb.212464
- Dubois, A. B., Cavagna, G. A. and Fox, R. S. (1974). Pressure distribution on the body surface of swimming fish. *J. Exp. Biol.* **60**, 581-591. doi:10.1242/jeb.60.3. 581
- Dubois, A. B. and Ogilvy, C. S. (1978). Forces on the tail surface of swimming fish: thrust, drag and acceleration in bluefish (*Pomatomus saltatrix*). J. Exp. Biol. 77, 225-241. doi:10.1242/jeb.77.1.225
- Elliott, J. M. and Davison, W. (1975). Energy equivalents of oxygen consumption in animal energetics. *Oecologia* 19, 195-201. doi:10.1007/BF00345305
- Eschmeyer, W. N. and Herald, E. S. (1999). A field guide to Pacific coast fishes: North America. Houghton Mifflin Harcourt.
- Esposito, C. J., Tangorra, J. L., Flammang, B. E. and Lauder, G. V. (2012). A robotic fish caudal fin: effects of stiffness and motor program on locomotor performance. *J. Exp. Biol.* **215**, 56-67. doi:10.1242/jeb.062711
- Feilich, K. L. and Lauder, G. V. (2015). Passive mechanical models of fish caudal fins: effects of shape and stiffness on self-propulsion. *Bioinspir. Biomim.* 10, 036002. doi:10.1088/1748-3190/10/3/036002
- Flammang, B. E. and Lauder, G. V. (2009). Caudal fin shape modulation and control during acceleration, braking and backing maneuvers in bluegill sunfish, *Lepomis macrochirus*. *J. Exp. Biol.* **212**, 277-286. doi:10.1242/jeb.021360
- Fletcher, T., Altringham, J., Peakall, J., Wignall, P. and Dorrell, R. (2014). Hydrodynamics of fossil fishes. *Proc. R. Soc. B* **281**, 20140703. doi:10.1098/rspb. 2014.0703
- Frith, H. R. and Blake, R. W. (1995). The mechanical power output and hydromechanical efficiency of northern pike (*Esox lucius*) fast-starts. *J. Exp. Biol.* 198, 1863-1873. doi:10.1242/jeb.198.9.1863
- Gemmell, B. J., Colin, S. P., Costello, J. H. and Dabiri, J. O. (2015). Suction-based propulsion as a basis for efficient animal swimming. *Nat. Commun.* **6**, 8790. doi:10.1038/ncomms9790
- Gemmell, B. J., Fogerson, S. M., Costello, J. H., Morgan, J. R., Dabiri, J. O. and Colin, S. P. (2016). How the bending kinematics of swimming lampreys build negative pressure fields for suction thrust. *J. Exp. Biol.* **219**, 3884-3895. doi:10. 1242/jeb.144642
- Gibb, A. C., Dickson, K. A. and Lauder, G. V. (1999). Tail kinematics of the chub mackerel *Scomber japonicus*: testing the homocercal tail model of fish propulsion. *J. Exp. Biol.* **202**, 2433-2447. doi:10.1242/jeb.202.18.2433
- **Graham, J. B. and Dickson, K. A.** (2004). Tuna comparative physiology. *J. Exp. Biol.* **207**, 4015-4024. doi:10.1242/jeb.01267
- Hansen, D. J. (1969). Food, growth, migration, reproduction, and abundance of pinfish, *Lagodon rhomboides*, and Atlantic croaker, *Micropogon undulatus*, near Pensacola. Florida. 1963–65. *Fish. Bull.* 68. 135-146.
- Helfman, G. S., Collette, B. B., Facey, D. E. and Bowen, B. W. (2009). The Diversity of Fishes: Biology, Evolution, and Ecology, 2nd edn. Hoboken, NJ: Wiley-Blackwell.
- Hunter, J. R. (1981). Feeding Ecology and predation of marine fish larvae. In Marine fish larvae (ed. R. Lasker), pp. 33-77. Seattle, WA: University of Washington Press
- Katzschmann, R. K., DelPreto, J., MacCurdy, R. and Rus, D. (2018). Exploration of underwater life with an acoustically controlled soft robotic fish. Sci. Robot. 3, eaar3449. doi:10.1126/scirobotics.aar3449
- Kendall, J. L., Lucey, K. S., Jones, E. A., Wang, J. and Ellerby, D. J. (2007).
  Mechanical and energetic factors underlying gait transitions in bluegill sunfish (*Lepomis macrochirus*). J. Exp. Biol. 210, 4265-4271. doi:10.1242/jeb.009498
- Kerschner, B. A., Peterson, M. S. and Gilmore, R. G. (1985). Ecotopic and ontogenetic trophic variation in mojarras (Pisces: Gerreidae). *Estuaries* 8, 311-322. doi:10.2307/1351492
- Korsmeyer, K. E., Steffensen, J. F. and Herskin, J. (2002). Energetics of median and paired fin swimming, body and caudal fin swimming, and gait transition in parrotfish (*Scarus schlegeli*) and triggerfish (*Rhinecanthus aculeatus*). J. Exp. Biol. 205, 1253-1263. doi:10.1242/jeb.205.9.1253
- Krishnadas, A., Ravichandran, S. and Rajagopal, P. (2018). Analysis of biomimetic caudal fin shapes for optimal propulsive efficiency. *Ocean Eng.* 153, 132-142. doi:10.1016/j.oceaneng.2018.01.082
- Lauder, G. V. (1982). Structure and function in the tail of the Pumpkinseed sunfish (Lepomis gibbosus). J. Zool. 197, 483-495. doi:10.1111/jzo.1982.197.4.483
- Lauder, G. V. (1989). Caudal fin locomotion in ray-finned fishes: historical and functional analyses. Am. Zool. 29, 85-102. doi:10.1093/icb/29.1.85
- Lauder, G. V. (2000). Function of the caudal fin during locomotion in fishes: kinematics, flow visualization, and evolutionary patterns. *Am. Zool.* 40, 101-122. doi:10.1093/icb/40.1.101
- Lauder, G. V. (2014). Fish locomotion: recent advances and new directions. Annu. Rev. Mar. Sci. 7, 521-545. doi:10.1146/annurev-marine-010814-015614
- Lauder, G. V. and Drucker, E. G. (2002). Forces, fishes, and fluids: hydrodynamic mechanisms of aquatic locomotion. *Physiology* 17, 235-240. doi:10.1152/nips. 01398.2002

- Lauder, G. V. and Drucker, E. G. (2004). Morphology and experimental hydrodynamics of fish fin control surfaces. *IEEE J. Oceanic Eng.* 29, 556-571. doi:10.1109/JOE.2004.833219
- Lauder, G. V. and Madden, P. G. A. (2007). Fish locomotion: kinematics and hydrodynamics of flexible foil-like fins. Exp. Fluids 43, 641-653. doi:10.1007/ s00348-007-0357-4
- Lauder, G. V., Flammang, B. and Alben, S. (2012). Passive robotic models of propulsion by the bodies and caudal fins of fish. *Integr. Comp. Biol.* 52, 576-587. doi:10.1093/icb/ics096
- Li, L., Nagy, M., Graving, J. M., Bak-Coleman, J., Xie, G. and Couzin, I. D. (2020).
  Vortex phase matching as a strategy for schooling in robots and in fish. *Nat. Commun.* 11, 5408, doi:10.1038/s41467-020-19086-0
- Liao, J. C. (2022). Fish swimming efficiency. Curr. Biol. 32, R666-R671. doi:10. 1016/j.cub.2022.04.073
- Liu, G. and Dong, H. (2016). Effects of tail geometries on the performance and wake pattern in flapping propulsion. In ASME 2016 Fluids Engineering Division Summer Meeting. Washington, DC, USA: American Society of Mechanical Engineers Digital Collection.
- Lucas, K. N., Johnson, N., Beaulieu, W. T., Cathcart, E., Tirrell, G., Colin, S. P., Gemmell, B. J., Dabiri, J. O. and Costello, J. H. (2014). Bending rules for animal propulsion. *Nat. Commun.* 5, 3293. doi:10.1038/ncomms4293
- Lucas, K. N., Dabiri, J. O. and Lauder, G. V. (2017). A pressure-based force and torque prediction technique for the study of fish-like swimming. PLoS ONE 12, e0189225. doi:10.1371/journal.pone.0189225
- Lucas, K. N., Lauder, G. V. and Tytell, E. D. (2020). Airfoil-like mechanics generate thrust on the anterior body of swimming fishes. *Proc. Natl. Acad. Sci. USA* 117, 10585-10592. doi:10.1073/pnas.1919055117
- Maertens, A. P., Triantafyllou, M. S. and Yue, D. K. P. (2015). Efficiency of fish propulsion. *Bioinspir. Biomim.* 10, 046013. doi:10.1088/1748-3190/10/4/046013
- Magnuson, J. J. (1966). Continuous locomotion in scombrid fishes. Am. Zool. 6, 503-504. doi:10.1093/icb/6.4.503
- Magnuson, J. J. (1970). Hydrostatic equilibrium of Euthynnus affinis, a pelagic teleost without a gas bladder. Copeia 1970, 56-85. doi:10.2307/1441976
- Müller, U. K., van den Heuvel, B. L. E., Stamhuis, E. J. and Videler, J. J. (1997).
  Fish footprints: morphology and energetics of the wake behind a continuously swimming mullet (*Chelon labrosus* Risso). *J. Exp. Biol.* 200, 2893-2906. doi:10. 1242/ieb.200.22.2893
- **Nelson, R. S.** (2002). Catch and release: a management tool for Florida. In American Fisheries Society Symposium, pp. 11-14.
- Neveln, I. D., Bai, Y., Snyder, J. B., Solberg, J. R., Curet, O. M., Lynch, K. M. and Maclver, M. A. (2013). Biomimetic and bio-inspired robotics in electric fish research. *J. Exp. Biol.* **216**, 2501-2514. doi:10.1242/jeb.082743
- Offen, N., Blum, N., Meyer, A. and Begemann, G. (2008). Fgfr1 signalling in the development of a sexually selected trait in vertebrates, the sword of swordtail fish. BMC Dev. Biol. 8, 98. doi:10.1186/1471-213X-8-98
- Reznick, D. N., Travis, J., Pollux, B. J. A. and Furness, A. I. (2021). Reproductive mode and conflict shape the evolution of male attributes and rate of speciation in the fish family Poeciliidae. *Front. Ecol. Evol.* 9, 639751. doi:10.3389/fevo.2021. 639751
- Rosic, M.-L. N., Thornycroft, P. J. M., Feilich, K. L., Lucas, K. N. and Lauder, G. V. (2017). Performance variation due to stiffness in a tuna-inspired flexible foil model. *Bioinspir. Biomim.* 12, 016011. doi:10.1088/1748-3190/aa5113
- Russo, T., Costa, C. and Cataudella, S. (2007). Correspondence between shape and feeding habit changes throughout ontogeny of gilthead sea bream Sparus aurata L., 1758. J. Fish Biol. 71, 629-656. doi:10.1111/j.1095-8649.2007.01528.x
- Saadat, M., Fish, F. E., Domel, A. G., Di Santo, V., Lauder, G. V. and Haj-Hariri, H. (2017). On the rules for aquatic locomotion. *Phys. Rev. Fluids* 2, 083102. doi:10. 1103/PhysRevFluids.2.083102
- Sagnes, P., Gaudin, P. and Statzner, B. (1997). Shifts in morphometrics and their relation to hydrodynamic potential and habitat use during grayling ontogenesis. *J. Fish Biol.* **50**, 846-858. doi:10.1111/j.1095-8649.1997.tb01977.x
- Sfakiotakis, M., Lane, D. M. and Davies, J. B. C. (1999). Review of fish swimming modes for aquatic locomotion. *IEEE J. Oceanic Eng.* 24, 237-252. doi:10.1109/ 48.757275
- Song, J., Zhong, Y., Du, R., Yin, L. and Ding, Y. (2021). Tail shapes lead to different propulsive mechanisms in the body/caudal fin undulation of fish. *Proc. Inst. Mech. Eng. C J. Mec.* 235, 351-364. doi:10.1177/0954406220967687
- Standen, E. M. and Lauder, G. V. (2005). Dorsal and anal fin function in bluegill sunfish *Lepomis macrochirus*: three-dimensional kinematics during propulsion and maneuvering. *J. Exp. Biol.* 208, 2753-2763. doi:10.1242/jeb.01706
- Stoner, A. W. (1980). Feeding ecology of Lagodon rhomboides (Pisces: Sparidae): variation and functional responses. Fish. Bull. 78, 337-352.
- Stoner, A. W. and Livingston, R. J. (1984). Ontogenetic patterns in diet and feeding morphology in sympatric sparid fishes from seagrass meadows. *Copeia* 1984, 174-187. doi:10.2307/1445050
- Tack, N. B., Du Clos, K. T. and Gemmell, B. J. (2021). Anguilliform locomotion across a natural range of swimming speeds. *Fluids* 6, 127. doi:10.3390/ fluids6030127

- Tangorra, J. L., Esposito, C. J. and Lauder, G. V. (2009). Biorobotic fins for investigations of fish locomotion. In 2009 IEEE/RSJ International Conference on Intelligent Robots and Systems, pp. 2120-2125.
- Tytell, E. D. (2006). Median fin function in bluegill sunfish *Lepomis macrochirus*: streamwise vortex structure during steady swimming. *J. Exp. Biol.* 209, 1516-1534. doi:10.1242/ieb.02154
- **Tytell, E. D.** (2007). Do trout swim better than eels? Challenges for estimating performance based on the wake of self-propelled bodies. *Exp. Fluids* **43**, 701-712. doi:10.1007/s00348-007-0343-x
- van Buren, T., Floryan, D., Brunner, D., Senturk, U. and Smits, A. J. (2017). Impact of trailing edge shape on the wake and propulsive performance of pitching panels. *Phys. Rev. Fluids* 2, 014702. doi:10.1103/PhysRevFluids.2.014702
- van Ginneken, V., Antonissen, E., Müller, U. K., Booms, R., Eding, E., Verreth, J. and van den Thillart, G. (2005). Eel migration to the Sargasso: remarkably high swimming efficiency and low energy costs. *J. Exp. Biol.* 208, 1329-1335. doi:10. 1242/jeb.01524
- Videler, J. J. (1977). Mechanical properties of fish tail joints. Fortschr. Zool 24, 183-194
- Videler, J. J. and Weihs, D. (1982). Energetic advantages of burst-and-coast swimming of fish at high speeds. *J. Exp. Biol.* **97**, 169-178. doi:10.1242/jeb.97.1. 169
- Wainwright, D. K. and Lauder, G. V. (2020). Tunas as a high-performance fish platform for inspiring the next generation of autonomous underwater vehicles. *Bioinspir. Biomim.* 15, 035007. doi:10.1088/1748-3190/ab75f7
- Wang, Y., Wang, R., Wang, S., Tan, M. and Yu, J. (2019a). Underwater bioinspired propulsion: From inspection to manipulation. *IEEE T. Ind. Electron.* **67**, 7629-7638. doi:10.1109/TIE.2019.2944082
- Wang, J., Tran, H., Christino, M., White, C., Zhu, J., Lauder, G., Bart-Smith, H. and Dong, H. (2019). Hydrodynamics and Flow Characterization of Tuna-Inspired Propulsion in Forward Swimming. In 8th ASME-JSME-KSME Joint Fluids

- Engineering Conference 2019. Volume 1: Fluid Mechanics, San Francisco, California, USA, July 28-August 1, 2019. p. V001T01A025. New York, N.Y: The American Society of Mechanical Engineers.
- **Webb**, **P. W.** (1975). Efficiency of pectoral-fin propulsion of *Cymatogaster aggregata*. In *Swimming and Flying in Nature* (ed. T. Y. T. Wu, C. J. Brokaw and C. Brennen), pp. 573-584. Springer.
- Webb, P. W. (1978a). Fast-start performance and body form in seven species of teleost fish. J. Exp. Biol. 74, 211-226. doi:10.1242/jeb.74.1.211
- Webb, P. W. (1978b). Hydrodynamics: Nonscombroid fish. In *Fish phisiology* (ed. W. S. Hoar and D. J. Randall), pp. 189-237. New York: Academic Press.
- Webb, P. W. (1992). Is the high cost of body/caudal fin undulatory swimming due to increased friction drag or inertial recoil? *J. Exp. Biol.* **162**, 157-166. doi:10.1242/jeb.162.1.157
- Webb, P. W. (2005). Stability and maneuverability. Fish Physiol. 23, 281-332. doi:10. 1016/S1546-5098(05)23008-X
- Weihs, D. (1973a). The mechanism of rapid starting of slender fish. Biorheology 10, 343-350. doi:10.3233/BIR-1973-10308
- Weihs, D. (1973b). Optimal fish cruising speed. *Nature* **245**, 48-50. doi:10.1038/ 245048a0
- White, C. H., Lauder, G. V. and Bart-Smith, H. (2021). Tunabot Flex: a tunainspired robot with body flexibility improves high-performance swimming. *Bioinspir. Biomim.* 16, 026019. doi:10.1088/1748-3190/abb86d
- Wilga, C. D. and Lauder, G. V. (2002). Function of the heterocercal tail in sharks: quantitative wake dynamics during steady horizontal swimming and vertical maneuvering. J. Exp. Biol. 205, 2365-2374. doi:10.1242/jeb.205.16.2365
- Zhu, J., White, C., Wainwright, D. K., Di Santo, V., Lauder, G. V. and Bart-Smith, H. (2019). Tuna robotics: A high-frequency experimental platform exploring the performance space of swimming fishes. *Sci. Robot.* **4**, eaax415. doi:10.1126/scirobotics.aax4615

# **Supplementary Materials and Methods**

## Comparison of Mojarra and Pinfish

Standard metabolic rate

The Mojarra and Pinfish specimens tested in this investigation displayed standard metabolic rates that did not show a strong statistical difference. Mean standard metabolic rate was equal to  $3.06\pm0.98$  and  $4.27\pm0.83$  mg min<sup>-1</sup> kg<sup>-1</sup> for Mojarras and Pinfish respectively (*t*-test, P = 0.055).

## Body aspect ratio

Measurements of body shapes for both fish species were obtained digitally for each specimen from scaled dorsal and lateral images of the fish using ImageJ software. Body width (w, thickness along left-right axis) was measured from dorsal views and body depth (d, height along ventral-dorsal axis) was measured from lateral views. Measurements were performed at the location along the rostro-caudal axis of the fish for which body depth was the greatest (Fig. S1A). From these, we calculated the aspect ratio of the body ( $AR_{body}$ ) using equation 1:

$$AR_{body} = \frac{w}{d} \tag{1}$$

The AR<sub>body</sub> of Mojarras and Pinfish showed no statistical diffrence and were equal to  $0.37\pm0.03$  and  $0.38\pm0.02$  respectively (*U*-test, P=0.53).

## Tail aspect ratio and sweep angle

Measurements of tail shape for Mojarras and Pinfish were obtained digitally for each specimen from scaled lateral iameges of the fish using ImageJ software. The span of the fin (h) was measured as the distance between the superior and inferior tips of the caudal fin. The surface area of the caudal fin (A) was measured as the portion of the tail defined by the presence of fin rays (Fig. S1B). The aspect ratio (AR) of the tail was calculated using equation 2:

$$AR = \frac{h^2}{A} \tag{2}$$

The sweep angle ( $\Lambda$ ) of the tail was measured in degrees as the angle formed by the leading edges of the superior and inferior sections of the tail (Fig. S1C)

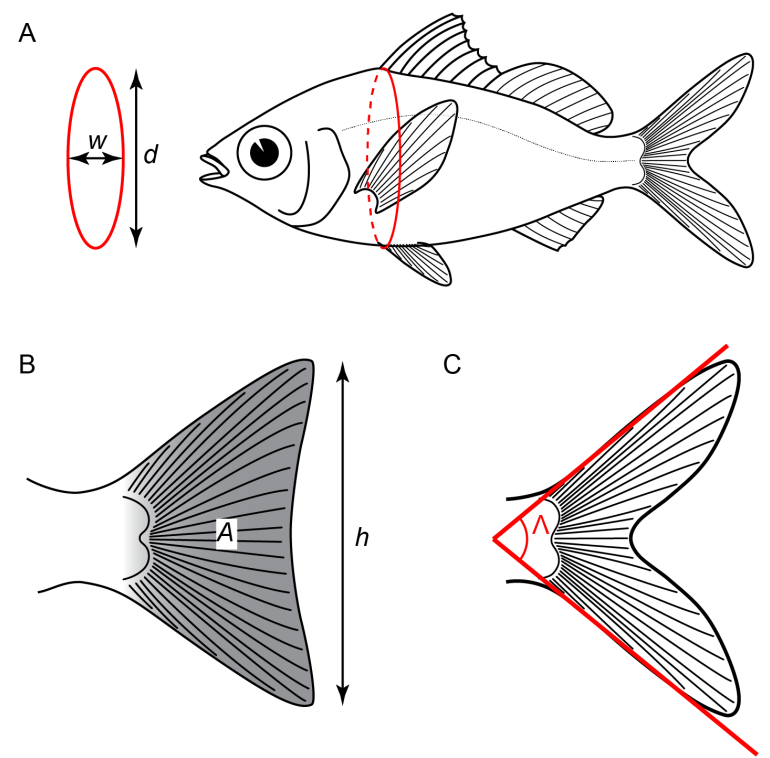


Fig. S1. Measurement of body morphology and tail geometry. (A) Body aspect ratio was calculated as the ratio of body width (w) to body depth (d). (B) Tail aspect ratio was computed as the ratio of the maximum theoretical surface area of the caudal fin given its height  $(h^2)$  to the actual measured fin surface area (A) represented by the gray shading. (C) The sweep angle  $(\Lambda)$  of the tail was measured as the angle formed by the leading edges of the superior and inferior sections of the tail. All measurements where performed using digital images of the fish.

# Determination of suitable experimental swimming speed

The COT of Mojarras and Pinfish followed a J-shaped trend, commonly reported in other species (Korsmeyer et al., 2002; Webb, 1975). Mojarras and Pinfish reached their optimal swimming speed  $U = 1.21 \text{ BL s}^{-1}$  and  $U = 1.99 \text{ BL s}^{-1}$  respectively where their COT was the lowest. A unique swimming speed  $U = 1.5 BL s^{-1}$  was selected for this study because it was representative of the optimal swimming speed at which the COT of both species were near their minima and the BCF mode of swimming was consistently displayed by the fish. The COT at this prescribed speed was  $3.831 \pm 1.543$  and  $1.789\pm0.683$  J m<sup>-1</sup> kg<sup>-1</sup> for Mojarras and Pinfish respectively (*U*-test, P = 0.032) and throughout the entire range of swimming speeds tested, the Mojarras exhibited a higher cost of transport (Fig. 7). These methods are further supported by the fact that most fish generally select their preferred swimming speed and swimming mode during cruising that correspond to the optimal swimming speed at which the COT is the lowest (Tudorache et al., 2011; Tudorache et al., 2013). This approach ensured that the performance of the forked and truncate tails, and the metabolic requirements of swimming for both species would be comparable not just based on the anatomy and kinematics of their caudal fins, but also by considering relevant ecological factors governing the behaviors of these species. Additionally, the range of swimming speeds that could be compared was limited by the sequential change in the gaits exhibited by the fish across swimming speeds. At speeds < 1.0 BL s<sup>-1</sup>, Mojarras and Pinfish

used their pectoral fins and caudal fin concurrently, thus likely distributing thrust production over these three propulsors. This swimming speed was deemed inadequate to compare the overall performance and energetics of using caudal fins with differing morphologies. At speeds > 2.0 BL s<sup>-1</sup>, Mojarras would begin exhibiting a behavior associated with burst and coast swimming rather than continuous and consistent BCF. Though this behavior would not manifest immediately, prolonged swimming causing this behavior eventually led to the increase in the COT due to fatigue. Consequently, we chose the swimming speed  $U = 1.5 \text{ BL s}^{-1}$  which yielded the same BCF mode of swimming in both species and equated to nearly equivalent optimal swimming speeds.

# Swim tunnel setup and laser sheet positioning

Individual fish naturally swam steadily at the center of the test section against the flow. One advantage of using visible laser light was that the fish always positioned themselves upstream of the vertical laser sheet and swam steadily in a predictable maner. The steadiness of the fish in the test section is further demonstrated by the very small surge displacement of the fish during several consecutive tail beats (see Figs 3,4). As such, the laser sheet could be positioned very precisely to intesect with the tail within less than two laser sheet widths (< 0.15 cm) on either side of the vertical axis located 2/3 of the tail length from the caudal peduncle. This corresponded to the vertical axis located at about 0.93 BL for both species. This location was chosen to fall within the center of the interlobar notch of the forked tail of Mojarras. For vertical planar transections of the tail (posterior view), a narrow mirror was mounted downstream of the swimming fish at a 45-degree angle to project the posterior view of tail to the camera mounted above (Fig. S2).

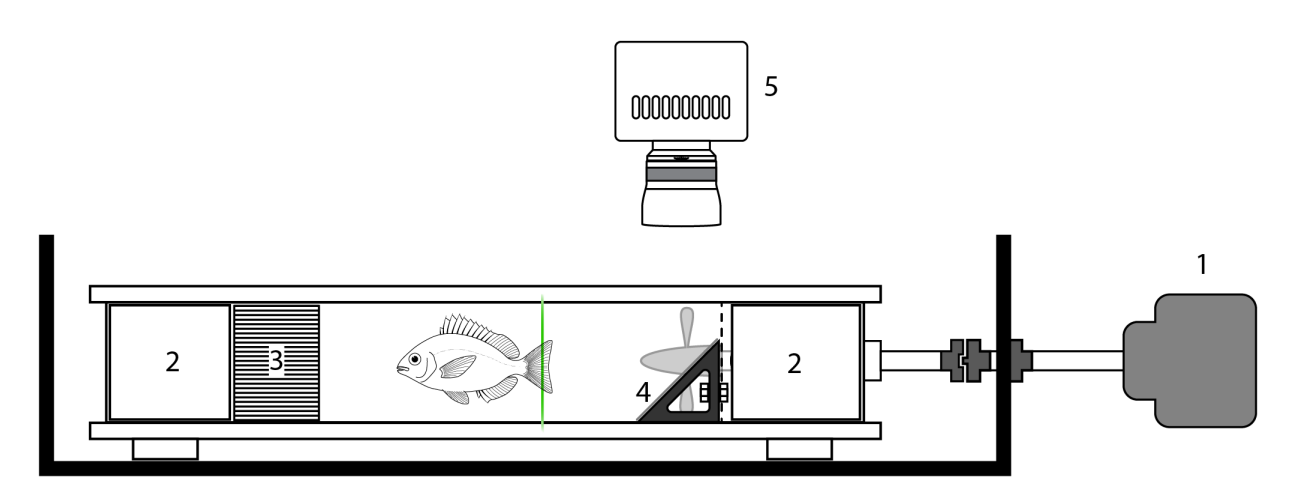


Fig. S2. Modified Brett-type swim tunnel respirometer used for particle image velocimetry (PIV) and respirometry experiments. Vertical transections of the tail required only one laser sheet (vertical green line). (1) motor, (2) flow straightener (vanes), (3) honeycomb flow straightener, (4) 45-degree angle mirror, (5) high-speed camera.

## Force calculations

Pressure fields were used to calculate gross thrust and drag forces per height along 150 evenly sized segments around the body by multiplying the pressure measured at the boundary of the fish by the length of each segment between points in a calculation boundary drawn around the fish, the unit vector normal to each segment, and the body depth at the location of each segments along the body. Specifically, thrust and drag were computed as the product of pressure, the area of the body segments defined by the width and heigh of each body boundary segment band, and the unit vector in the direction of swimming. Thrust forces are positive and drag forces are negative. To simplify terminology, forces were classified as pull and push forces when arising from sub-ambient pressures (negative relative to ambient) and above-ambient pressures (positive), respectively.

# Forked tail deformation across swimming speeds

The cupping pattern observed in the forked caudal fin was observed across multiple sustained swimming speeds surrounding the optimal swimming speed of the fish (Fig. S3). This cupping pattern was caused by the superior and inferior edges of the fin lobes leading the tail beat while their center was lagging. The cupping of the lobes was generally symmetrical about the midline of the fish and showed little variation between the two phases of a complete tail beat. Both lobes showed identical patterns.

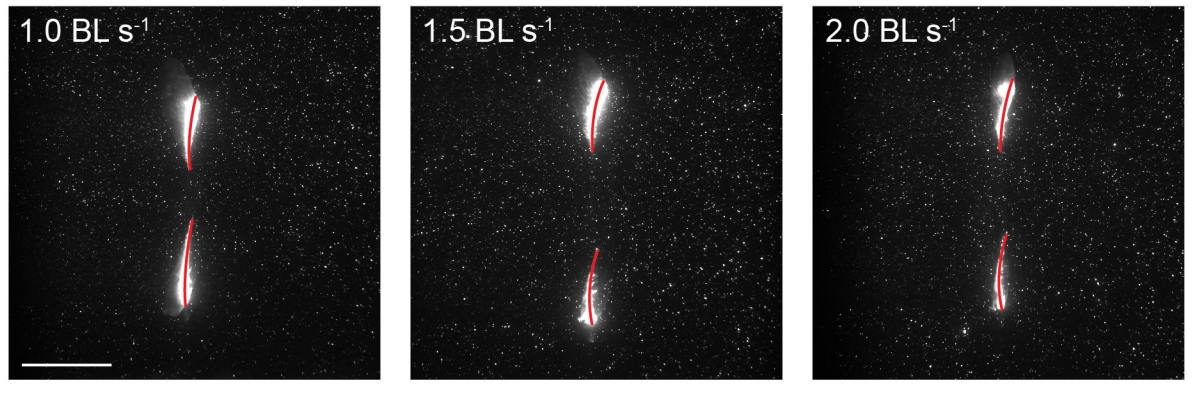


Fig. S3. Vertical transections during mid tail stroke for one representative fish swimming at 1.0, 1.5, and 2.0 BL s<sup>-1</sup>. Red curved lines indicate emphasize the deformation of the lobes along the vertical plane. Scale bar represents 1 cm for all frames.

## Fin kinematics and force production

Fast Fourier transforms (FFT) were performed on tail displacement, fin angle and surge thrust over time for both the Mojarras and Pinfish using a custom program in MATLAB R2020a. This function computed the discrete Fourier transform (DFT) of these data using a FFT algorithm. Previous studies predicting the forces generated by oscillating tail analogs indicate that the frequency of thrust and drag cycles during a complete tail beat is twice that of frequency of the motions of the tail (Esposito et al., 2012; Xiong and Lauder, 2014). Both species displayed a similar pattern. Tail-beat and fin angle had matching frequencies, that were half that of the thrust and drag cycles occurring during a full tail beat.

## Pressure fields across the tail

The magnitude of the sub-ambient and positive pressure fields generated on either side of the forked tail of the Mojarras was less than that of the truncate tail (Fig. S4, U-test, P < 0.01). Peak positive and negative pressures were averaged for the left and right sides of the fin during the two halves of a complete tail beat.

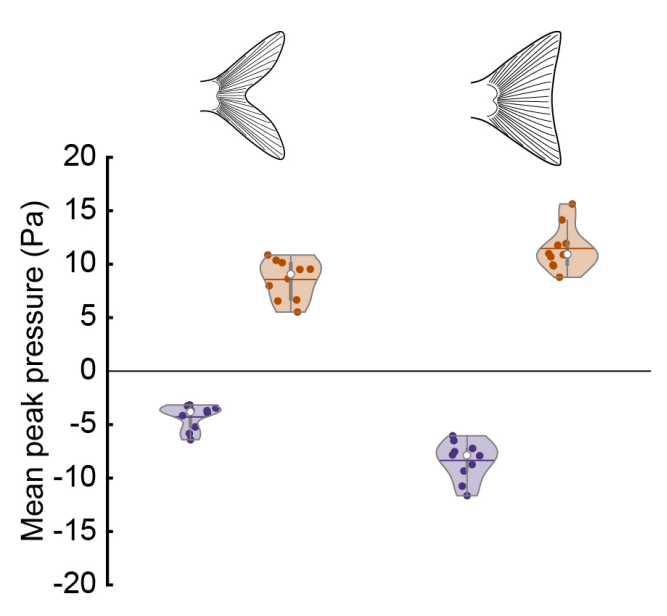


Fig. S4. Mean peak pressures measured on either side of the caudal fin during a tail beat. Both fish were swimming at the same relative swimming speed  $U = 1.5 \text{ BL s}^{-1}$ . The magnitude of the sub-ambient (purple) and positive (orange) pressure fields generated during tail lateral displacement were significantly different between the two tail types (*U*-tests; sub-ambient P < 0.001, positive P = 0.005).

# Calculation of the coefficient of pressure and thrust

Coefficient of pressure and thrust ( $C_p$  and  $C_{Fx}$ ) were calculated to compare the effectiveness of the two tail morphologies in generating thrust. While direct measurement of the magnitude of the forces produced by the two tail types is more suitable to comparing the fundamental differences in performance, these non-dimensional coefficients provide more useful insights about how tail shape may or may not fundamentally affect how forces are produced. These coefficients were calculated as follows based on the methods by Lucas et al. (2020):

$$C_p = \frac{p}{\frac{1}{2}\rho u_{tail}^2} \tag{3}$$

$$C_{F_{\chi}} = \frac{F_{\chi}}{\frac{1}{2}\rho A u_{tail}^2} \tag{4}$$

where  $C_p$  is pressure coefficient, p is pressure (Pa),  $C_{Fx}$  is thrust coefficient (force in the swimming direction),  $F_x$  is thrust (N), p is the density of 30% water at 21°C (1020.7 kg m<sup>-3</sup>), u is the lateral speed of the tail (m s<sup>-1</sup>), and A is the lateral area of the fish's tail (m<sup>2</sup>).

# Comparison of flexible forked tail and lunate tail

The lunate tail is characterized by its undeformable tapered hydrofoil profile with a straight chord (Fig 8A, red line). This contrasts with the tail of Mojarras that is pliable and whose surface configuration forms a cupping pattern during lateral excursions. The pitching and heaving motions of the lunate tail causes the superior and inferior edges of the fin to lead the lateral motion, while the trailing edges formed by the fork are lagging (Fig 8B). In contrary, because of the cupping of the fin lobes of the Mojarra's caudal fin, both the leading and trailing edges are leading during a tail beat (Fig. 8C, D). This specific conformation was identified from the raw PIV videos as the tail was illuminated by the vertical laser sheet. In the rigid lunate tail, the LEV remains attached to the surface of the fin. The TEV separates from the trailing edge and only re-attaches upon tail reversal. Contrary to the lunate tail, the LEV of the flexible tail remains attached to the leading edge but does not extend over the surface of the fin. The TEV shows a similar pattern.

# Asymmetry of the Mojarra's fin lobes during vertical maneuvers

Although a full analysis of the orientation of the fin lobes along the vertical axis and its effects on maneuverability was not the focus of this study, we noted that the superior and inferior tail lobes were not kept at equal angles relative to the direction of swimming during occasional vertical repositioning in the swim tunnel (Fig. S5). The increase of the angle formed by the inferior caudal lobe and a slight decrease in the angle formed by the superior lobe cause the fish to pitch upward (t = 0-0.75 s). At the end of this maneuver, the angle formed by both lobes is almost equal (t = 1.5 s). Angles were measured using ImageJ-Fiji. The resulting changes in depth did not require the use on any other fins. The steering capabilities offered by conformational changes of the homocercal tail of teleost has never been demonstrated but studies found that during cruising, the superior lobe of the heterocercal tail of sharks produces downward and posteriorly oriented forces to maintain vertical postural stability (Wilga and Lauder, 2002). Though we did not assess the hydrodynamic effects of transient asymmetries in forked fins during cruising, it is likely that a similar mechanism be employed to control pitch such that the fish can maneuver along the vertical plane without the use of other fins.

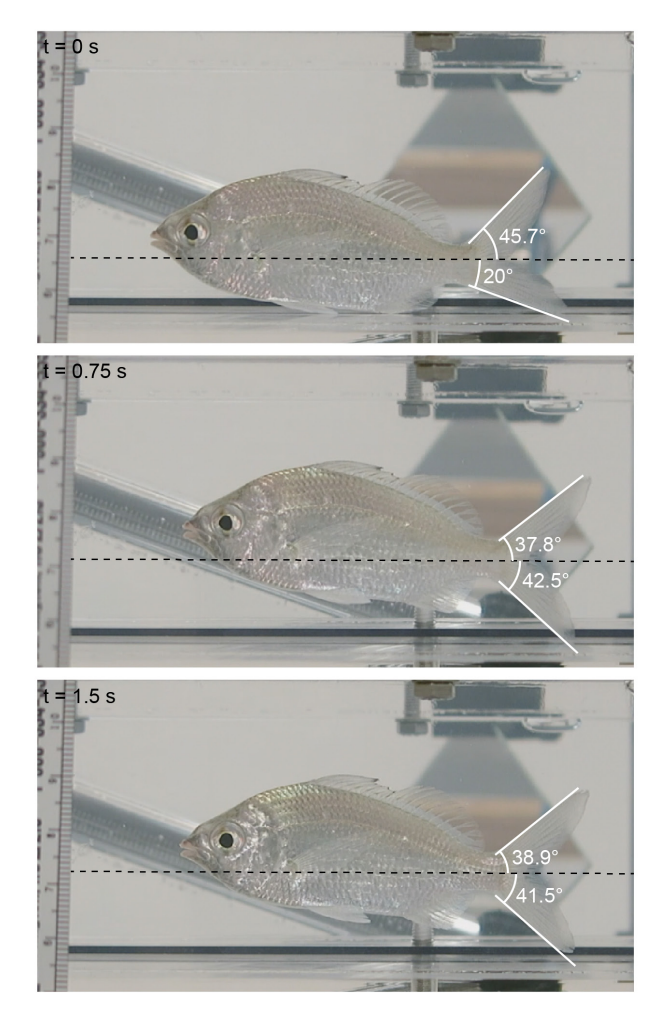


Fig. S5. Asymmetrical conformation of the forked fin lobes during vertical repositioning at a cruising speed of 1.0 BL  $\rm s^{-1}$ . Changes in the angles formed by the leading edges of the fin lobes (white lines) relative to direction of swimming (black dashed line) corresponded to a change in the vertical position of the fish in the test section (see ruler on the left).

# References

- Esposito, C. J., Tangorra, J. L., Flammang, B. E. and Lauder, G. V. (2012). A robotic fish caudal fin: effects of stiffness and motor program on locomotor performance. *J. Exp. Biol.* 215, 56–67.
- **Korsmeyer, K. E., Steffensen, J. F. and Herskin, J.** (2002). Energetics of median and paired fin swimming, body and caudal fin swimming, and gait transition in parrotfish (*Scarus schlegeli*) and triggerfish (*Rhinecanthus aculeatus*). *J. Exp. Biol.* **205**, 1253–1263.
- Lucas, K. N., Lauder, G. V. and Tytell, E. D. (2020). Airfoil-like mechanics generate thrust on the anterior body of swimming fishes. *P. Natl. Acad. Sci.* 117, 10585–10592.
- **Sfakiotakis, M., Lane, D. M. and Davies, J. B. C.** (1999). Review of fish swimming modes for aquatic locomotion. *IEEE J. Oceanic Eng.* **24**, 237–252.

- **Tudorache, C., O'Keefe, R. A. and Benfey, T. J.** (2011). Optimal swimming speeds reflect preferred swimming speeds of brook charr (*Salvelinus fontinalis* Mitchill, 1874). *Fish Physiol. Biochem.* **37**, 307–315.
- **Tudorache, C., de Boeck, G. and Claireaux, G.** (2013). Forced and preferred swimming speeds of fish: a methodological approach. In *Swimming Physiology of Fish* (ed. Arjan P. Palstra and Planas, J. V.), pp. 81–108. Berlin, Heidelberg: Springer.
- Wang, J., Tran, H., Christino, M., White, C., Zhu, J., Lauder, G., Bart-Smith, H. and Dong, H. (2019). Hydrodynamics and flow characterization of tuna-inspired propulsion in forward swimming. In *Fluids Engineering Division*, p. V001T01A025. American Society of Mechanical Engineers.
- **Webb, P. W.** (1975). Efficiency of pectoral-fin propulsion of *Cymatogaster aggregata*. In *Swimming and flying in nature*, pp. 573–584. Springer.
- Wilga, C. D. and Lauder, G. V. (2002). Function of the heterocercal tail in sharks: quantitative wake dynamics during steady horizontal swimming and vertical maneuvering. *J. Exp. Biol.* **205**, 2365–2374.
- **Xiong, G. and Lauder, G. V.** (2014). Center of mass motion in swimming fish: effects of speed and locomotor mode during undulatory propulsion. *Zoology* **117**, 269–281.
- Zhu, J., White, C., Wainwright, D. K., Santo, V. D., Lauder, G. V. and Bart-Smith, H. (2019). Tuna robotics: A high-frequency experimental platform exploring the performance space of swimming fishes. *Sci. Robot.* 4, eaax415.